Project Report
TIP-61

Hierarchical Materials: Modeling, Manufacturing, and Testing of Lightweight Metals with Zero and Tunable Thermal Expansion: FY17 Engineering Research Technical Investment Program

E.M. Parsons

13 February 2018

Lincoln Laboratory
MASSACHUSETTS INSTITUTE OF TECHNOLOGY
LEXINGTON, MASSACHUSETTS

This material is based upon work supported by the Department of the Air Force
under Air Force Contract FA8721-05-C-0002 and/or FA8702-15-D-0001.

This report is the result of studies performed at Lincoln Laboratory, a federally funded research and development center operated by Massachusetts Institute of Technology. This material is based upon work supported under Air Force Contract No. FA8721-05-C-0002 and/or FA8702-15-D-0001. Any opinions, findings, conclusions or recommendations expressed in this material are those of the author(s) and do not necessarily reflect the views of the Assistant Secretary of Defense for Research and Engineering.

Massachusetts Institute of Technology
Lincoln Laboratory

Hierarchical Materials: Modeling, Manufacturing, and Testing of Lightweight Metals with Zero and Tunable Thermal Expansion: FY17 Engineering Research Technical Investment Program

E.M. Parsons
Group 74

Project Report TIP-61

13 February 2018

This material is based upon work supported by the Department of the Air Force under Air Force Contract FA8721-05-C-0002 and/or FA8702-15-D-0001.

Lexington Massachusetts

This page intentionally left blank.

ABSTRACT

A particularly challenging yet common problem at MIT Lincoln Laboratory is designing prototypes to function under repeated variations of temperature. Thermal expansion of components causes separation and alignment errors in optical systems, and stresses due to mismatches of thermal expansion at material interfaces cause fatigue and failure of components and structures. In addition to managing thermal expansion, minimizing system weight and maintaining short production cycles are critical requirements. However, presently available materials with low thermal expansion either are heavy or are expensive with long fabrication lead times. Furthermore, existing materials have essentially fixed thermal expansions and provide only limited freedom to tune the response to the requirements of an application. These materials are solid materials with properties determined primarily by their elemental composition and microstructure. Here, we take a different approach and engineer materials by specifying underlying structure at one or more hierarchical levels to create materials with zero and tunable thermal expansion and high specific stiffness. Analytical and numerical models are used to design lattice-based cellular materials composed of two constituent materials with dissimilar thermal expansions. The lattice geometry and layout of constituent materials can be chosen to achieve zero or otherwise specified thermal expansion while maximizing specific stiffness, subject also to the constraints of automated manufacturing. Samples were manufactured with 3D printing and computer-controlled machining, and thermal expansion was measured with a novel optical method. The experimental results show effective thermal expansions ranging from $-14.0 \times 10^{-6}\,\mathrm{K}^{-1}$ to $17.1 \times 10^{-6}\,\mathrm{K}^{-1}$, demonstrating that we have developed the first metals with zero and tunable thermal expansion (to our knowledge) that can be manufactured with automated methods at useful scales. Moreover, the structural performance indices of these materials are predicted to exceed the indices of conventional aerospace materials, in some cases even approaching the theoretical upper bound for stiffness. As such, these materials have the potential to improve thermal stability, increase stiffness, reduce weight, and extend service life for many components and structures in sensor and communication systems.

This page intentionally left blank.

TABLE OF CONTENTS

This page intentionally left blank.

LIST OF FIGURES

LIST OF FIGURES
(Continued)

LIST OF FIGURES
(Continued)

LIST OF FIGURES
(Continued)

LIST OF FIGURES
(Continued)

LIST OF FIGURES
(Continued)

1. INTRODUCTION

Conventional engineering materials have been developed over many years by changing the chemistry or manipulating the processing conditions of existing materials. Although these methods slowly continue to enhance material properties, returns are diminishing, and therefore new approaches are now required to attain large improvements in material properties. The goal of this project was to develop materials with properties that are determined by underlying structure, not just elemental composition. These materials are frequently referred to as "metamaterials" because they can exhibit properties not commonly found in materials given to us by nature—such as extremely low density, negative Poisson's ratio, negative stiffness, frequency band gaps, and zero thermal expansion.

A difficult but common problem at MIT Lincoln Laboratory (MIT LL) is managing thermal expansion of materials without adding excessive weight to a component or structure or sacrificing design flexibility. Thermal expansion of materials can cause separation and alignment errors in optical systems, and stresses due to mismatches of thermal expansion at material interfaces can cause fatigue and failure of components and structures. Furthermore, aerospace applications also require materials with high specific stiffness so that weight can be minimized, increasing performance and reducing the need for complex vibration isolation systems. Current solutions include using Invar, silicon carbide, or fiber-reinforced composites. Invar is heavy and exhibits low thermal expansion only over a limited range of temperature. Silicon carbide and fiber-reinforced composites are brittle, expensive, and difficult to fabricate into the complex geometries required for many MIT LL prototypes. Furthermore, all these materials essentially have fixed properties; their properties cannot be tailored to the requirements of a specific application (with the exception of fiber-reinforced composites to a limited extent). As such, there is a pressing need for lightweight, readily shaped structural materials that exhibit zero and tunable coefficients of thermal expansion (CTEs).

We propose to meet this need for zero and tunable CTE materials with two types of composite lattice material, each constructed from two easily machined metals with substantially differing CTEs. The superposition of materials with unequal CTEs can result in an effective CTE significantly lower than that predicted by the rule of mixtures. It is even possible for a composite material composed of constituent materials with positive CTEs to exhibit a negative effective CTE. However, zero or low thermal expansion cannot be achieved by simply combining two different solid materials. The underlying structure of each constituent phase must be specified at one or more hierarchical levels to cause the desired effective response. In this document, we describe the modeling, manufacturing, and testing of zero and tunable CTE materials that can be readily fabricated from 3D printed metals.

The remainder of this document is organized as follows: Section 2 introduces the concept of controlling thermal expansion by combining materials with dissimilar thermal expansions in the form of lattice-based cellular materials and describes the mechanics underlying the effective response of both hexagonal and triangular lattice materials. Section 3 describes the analytical and

numerical models that are used to explore, predict, and tune the thermal and mechanical responses of the composite lattice materials. Section 4 describes the manufacturing of these materials and the method of measuring thermal expansion. Section 5 presents both the modeling results and the experimental results. The design of a hexagonal lattice material with zero thermal expansion and maximized specific stiffness is described. Predictions of thermal expansion are compared with measurements, and the effect on thermal expansion of the width, thickness, and layer composition of the material sample are investigated with numerical simulations. Section 6, the conclusion of the document, briefly summarizes the success and novelty of this year's work and provides perspective on how the methods communicated in this document could be used for applications other than controlling thermal expansion.

2. CONCEPT: COMPOSITE LATTICE MATERIALS AND STRUCTURES WITH ZERO AND TUNABLE THERMAL EXPANSION

In this project, we designed, manufactured, and tested two types of composite lattice material that can exhibit zero and tunable thermal expansion. Both types of lattice material are composed of two constituent materials with dissimilar CTEs, but the mechanisms that prevent or control the thermal expansion of these materials are not the same. In one type of lattice material, the high CTE and low CTE constituent materials are arranged in alternating layers. During an increase in temperature, the expansion of the high CTE material in the plane of the layers causes the low CTE material to contract in the direction normal to the plane such that the overall expansion is zero in the transverse direction (Figure 1). Within each layer, we arrange the constituent material into a hexagonal lattice geometry that is designed to eliminate thermal expansion and maximize specific stiffness. In the second type of lattice material, the two constituent materials are arranged into a triangular lattice geometry. When the temperature is increased, some elements bend and rotate into the void space of the material, counteracting the thermal expansion of the solid materials to an extent that the overall dimensions of the bulk material do not change.

For the solid material phases, aluminum and titanium were chosen because they exhibit excellent specific stiffnesses and substantially different CTEs. Furthermore, recent advances in 3D printing enable robust, automated fabrication of composites of aluminum and titanium at high resolution ($< 50\mu$m) by ultrasonic additive manufacturing. Aluminum and titanium are also easy to machine, causing post processing to be quick and simple.

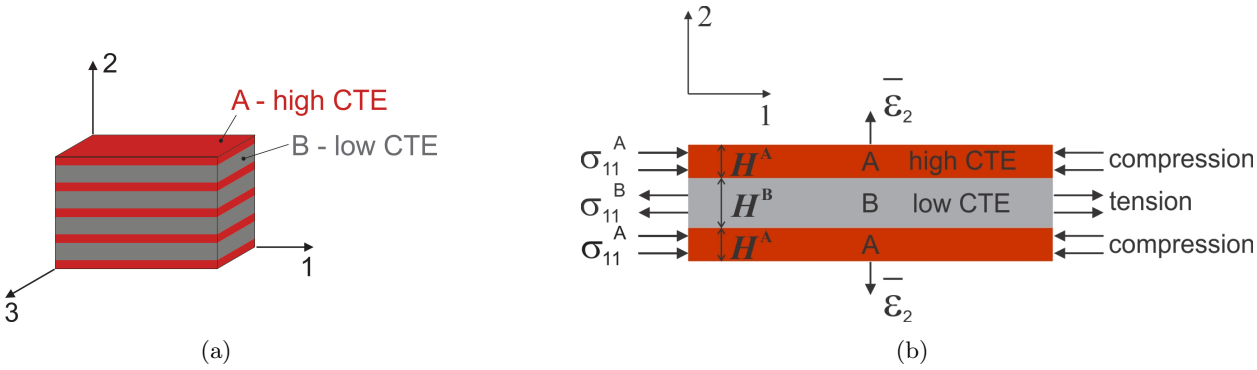

Figure 1. Model composite material composed of isotropic layers with contrasting coefficients of thermal expansion (CTEs): (a) High CTE layers and low CTE layers are stacked alternately and bonded to one another; (b) As a result, when subject to an increase in temperature, the low CTE layers are in tension and the high CTE layers are in compression (at the interior of the plate), causing the overall thermal expansion, $\bar{\epsilon}_{22}$, to be a function also of the elastic properties.

2.1 CONTROLLING THERMAL EXPANSION WITH COMPOSITE HEXAGONAL LATTICE MATERIALS

When two materials with contrasting thermal expansions are bonded together in layers, the effective thermal expansion of the composite material can, in some directions, be substantially lower than the thermal expansion of either constituent material. The effective thermal expansion is determined not only by the CTEs of the constituent materials but also by their elastic constants because the Poisson's ratio couples the principal elastic strains. However, attaining zero thermal expansion by this mechanism requires constituent materials with elastic properties well outside the bounds of isotropic metallic solids (i.e., Poisson's ratios beyond the thermodynamic limits, $-1 \leq \nu \leq 0.5$, and materials with both high CTE and high Young's modulus, two properties that are typically inversely related).

In order to achieve zero thermal expansion, we must use anisotropic materials, for which there are no bounds on Poission's ratio in general. Our solution is to design a lattice-based cellular material for each layer. Lattice-based cellular materials are regular arrangements of solid struts or plates in space that form the edges or faces of cells. By specifying the geometry of the solid material, we can precisely control the effective Poisson's ratio, stiffness, density, and strength of the cellular material. In particular, we choose a planar honeycomb that is constructed by tessellating a hexagonal unit cell throughout space (Figure 2). The elastic constants of this lattice material are strongly dependent on the geometry of the hexagonal unit cell (Figure 3). For example, a regular honeycomb material (cell wall internal angle $\theta = 30°$, $h = l$) possesses three axes of symmetry in the 1-2 plane and is therefore isotropic in the plane with a Poisson's ratio $\nu_{ij} \approx 1$. However, when $\theta \neq 30°$, the structure is no longer isotropic in the plane, and four independent elastic constants now characterize the in-plane deformation. Furthermore, when the cell wall internal angle, θ, is less than zero, the in-plane Poisson's ratios, ν_{ij} ($i = 1, 2,\ j = 1, 2$), become negative, causing the material to contract in the i-direction when compressed in the j-direction ($i \neq j$) and vice-versa ("bow tie" or re-entrant geometry, as shown in Figure 3b). This response is termed *auxetic* behavior. When combined in the form of a layered composite material, these anisotropic hexagonal materials enable broad tuning of the effective thermal expansion because they can exhibit Poisson's ratios far outside the limits of isotropic, homogeneous materials. In this work, we build the hexagonal lattice layers from either aluminum or titanium, two materials with a ratio of thermal expansions of nearly three.

A fundamental requirement for this type of zero CTE material is that the thickness of each layer in the 2-direction should be significantly smaller than the overall width of the material sample in the 1-direction. Otherwise, the absence of constraint at the free surfaces will limit the magnitude of the Poisson effect. Because the height of the unit cell of each constituent material can be no greater than its layer thickness (and it can be smaller), the unit cells must also be significantly smaller than the width of the sample. For this reason, we can consider the sample to be a "material," rather than a "structure" because the characteristic length of its underlying structure (the hexagonal unit cells) is much smaller than the width of the sample.

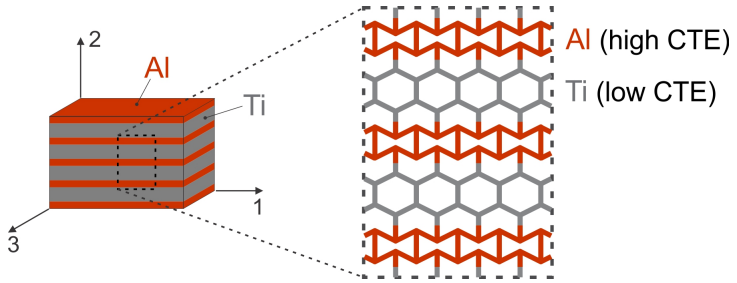

Figure 2. Hexagonal lattice material for controlling thermal expansion: Each layer of this layered composite material consists of hexagonal cells of aluminum (high CTE) or titanium (low CTE).

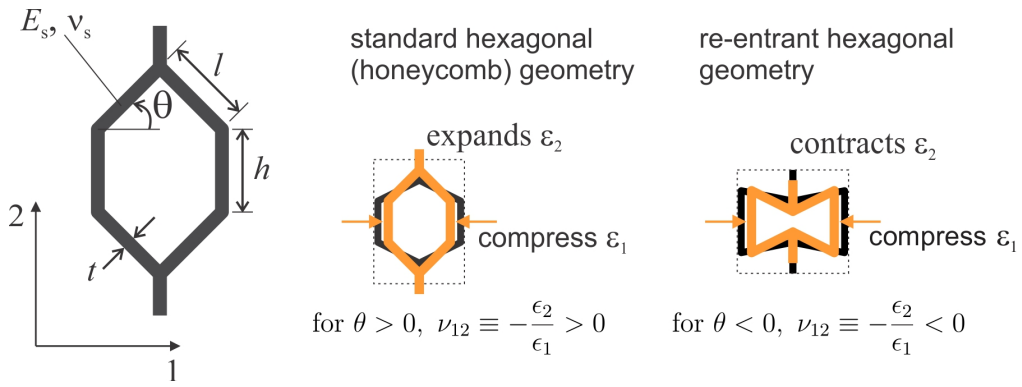

Figure 3. Hexagonal lattice materials: For positive cell wall internal angles, θ, the Poisson's ratios are positive, and the material expands in the 2-direction when compressed in the 1-direction; for negative cell wall internal angles, the Poisson's ratios are negative, and the material contracts in the 2-direction when compressed in the 1-direction (auxetic response).

2.2 CONTROLLING THERMAL EXPANSION WITH COMPOSITE TRIANGULAR LATTICE STRUCTURES

The second method to achieve zero thermal expansion with a dual material composite relies on bending of the struts or cell walls of lattice-based materials. Within each unit cell of the material, elements composed of a high CTE material cause other elements to rotate by bending into the interior space of the unit cell. When the change in a given unit cell dimension caused by rotation exactly compensates for the thermal expansion of the solid materials, the unit cell exhibits zero thermal expansion in the direction of that dimension. Here, we use a triangular unit cell with a base constructed from the high CTE material and legs constructed from the low CTE material. Subject to an increase of temperature, the expansion of the base of the triangle can cause the legs to rotate such that the height of the unit cell remains constant or decreases (Figure 4a). The change

in height of the unit cell, and therefore the thermal expansion in the 2-direction, $\overline{\alpha}_2$, is determined entirely by the relative thermal expansions of the two materials and the cell wall internal angle, θ. For the case of aluminum and titanium constituent materials, $\overline{\alpha}_2$ can be tuned to be zero, positive, or negative, simply by verifying θ.

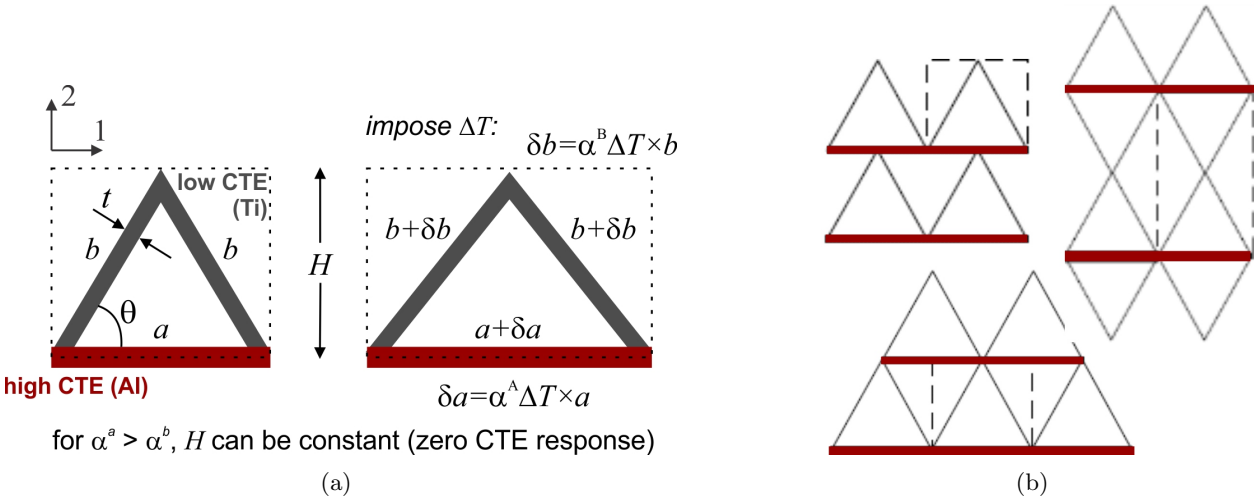

Figure 4. Triangular lattice structures for controlling thermal expansion: (a) The expansion of the base of the triangle can cause rotation of the legs of the triangle such that the structure does not expand (or contract) in the 2-direction; (b) Tessellation of the triangular unit cell in two dimensions creates various types of planar cellular structure. The structure at the bottom is the most structurally efficient because it is fully triangulated ($Z = 6$).

A benefit of this method for controlling thermal expansion is that the response does not depend on the scale of the material or structure. The mechanism that provides control of thermal expansion operates entirely within a single unit cell and does not rely on constraint stresses supplied by adjoining layers. In fact, when the joints of the unit cell are approximated as pin joints, then the unit cell deforms freely, without stress, during a change of temperature. Therefore, the thermal response of the unit cell is identical to that of any material or structure formed by tessellating the unit cell throughout space. Because we manufactured samples consisting of just a handful of cells, we hereon refer to the composite triangular samples as "structures" rather than materials. In an application, the size of the unit cell would be specified to be substantially smaller than the wavelength of the mechanical loading so that the load would be distributed continuously across multiple joints.

The triangular unit cell can be used as the building block for several different types of cellular structure (Figure 4b). These structures all exhibit identical thermal expansion, but their responses to mechanical loading are a function of the average nodal connectivity, Z, of the underlying lattice geometry. The fully triangulated lattice geometry at the bottom of Figure 4b has the highest nodal connectivity, $Z = 6$, and its pin jointed counterpart exhibits no collapse mechanisms. As a result, it accommodates mechanical loading in a highly efficient manner, primarily by extension and compression of its cell walls. The fully triangulated lattice geometry thus has the potential to provide both zero thermal expansion and exceptionally high specific stiffness.

This page intentionally left blank.

3. MODELING OF MATERIALS AND STRUCTURES WITH ZERO AND TUNABLE THERMAL EXPANSION

We developed both analytical and numerical models to investigate, predict and control the thermomechanical response of the composite lattice materials described in the previous section. For inputs, the models require only the properties of the two solid metals with contrasting CTEs (aluminum and titanium), the geometry of the underlying lattice, and the constraints of the ultrasonic additive manufacturing process.

3.1 ANALYTICAL MODELING OF COMPOSITE LATTICE MATERIALS AND STRUCTURES

Analytical models were developed for both types of composite lattice material in order to explore the efficacy of the designs and to enable rapid execution of parametric studies. The parametric studies elucidate the effect on thermomechanical performance of unit cell geometry, material density, and the width and thickness of the sample. The models can therefore predict which sets of parameters will result in materials or structures with zero (or otherwise specified) thermal expansion and maximized structural performance indices.

3.1.1 Analytical modeling of composite hexagonal lattice materials

The effective thermal expansion in the transverse direction of a layered composite material can be substantially less than the thermal expansion of either constituent material because the principal elastic strains are connected by the elastic constants of the constituent materials. During an increase of temperature, if the total elastic strain in the transverse direction (2-direction) caused by the Poisson contraction is equal to the total thermal strain, then the material does not change dimension in that direction. In the modeling of this effect, when each layer is composed of an anisotropic hexagonal lattice material, we make the following assumptions (Figure 5):

- Isotropic, elastic solid materials with Young's moduli $E_{\mathrm{s}}^{\mathrm{A}}$ and $E_{\mathrm{s}}^{\mathrm{B}}$, Poisson's ratios $\nu_{\mathrm{s}}^{\mathrm{A}}$ and $\nu_{\mathrm{s}}^{\mathrm{B}}$, and coefficients of thermal expansion $\alpha_{\mathrm{s}}^{\mathrm{A}} > \alpha_{\mathrm{s}}^{\mathrm{B}}$.
- Elastic hexagonal lattice materials with orthotropic compliances $C_{ij}^{\mathrm{A}}\left(E_{\mathrm{s}}^{\mathrm{A}}, \nu_{\mathrm{s}}^{\mathrm{A}}, \theta^{\mathrm{A}}, \frac{h^{\mathrm{A}}}{l^{\mathrm{A}}}, \frac{t^{\mathrm{A}}}{l^{\mathrm{A}}}\right)$ and $C_{ij}^{\mathrm{B}}\left(E_{\mathrm{s}}^{\mathrm{B}}, \nu_{\mathrm{s}}^{\mathrm{B}}, \theta^{\mathrm{B}}, \frac{h^{\mathrm{B}}}{l^{\mathrm{B}}}, \frac{t^{\mathrm{B}}}{l^{\mathrm{B}}}\right)$ and isotropic thermal expansions $\alpha^{\mathrm{A}} = \alpha_{\mathrm{s}}^{\mathrm{A}} > \alpha^{\mathrm{B}} = \alpha_{\mathrm{s}}^{\mathrm{B}}$. (Refer also to Figure 3.)
- The width of the material in the 1-direction is significantly greater than the thicknesses of each layer so that the effect of the free surfaces can be neglected, permitting the use of periodic boundary conditions.

- The material consists of an odd number of layers so that no bending occurs or, alternatively, the sample consists of many layers.
- Each layer is perfectly bonded to its adjoining layers.
- The temperature is uniform throughout the material.

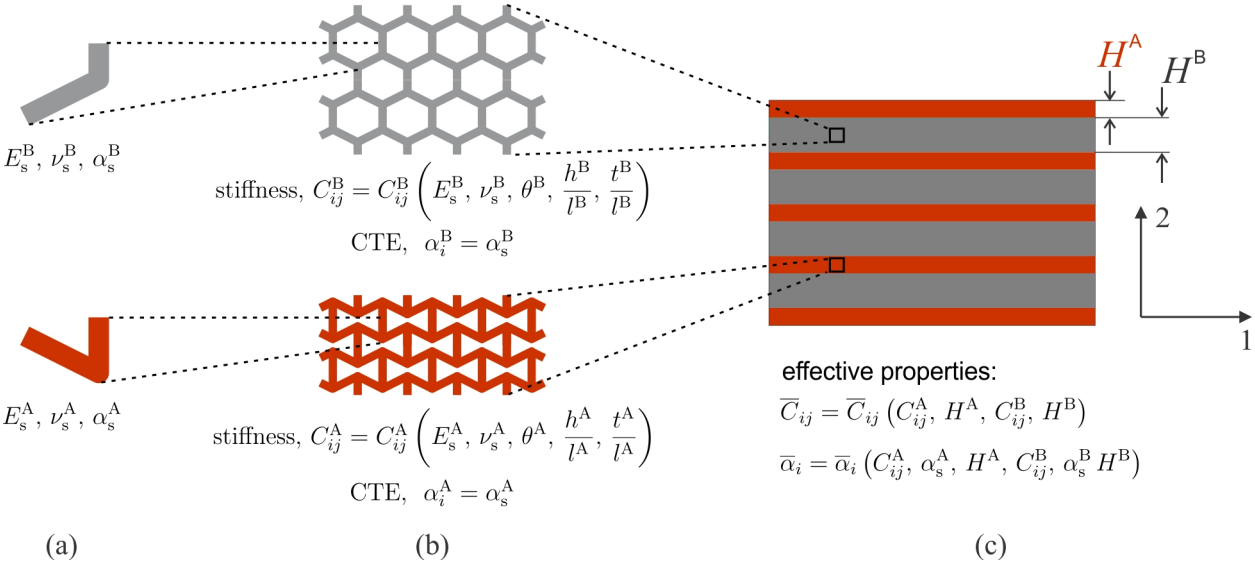

Figure 5. Analytical modeling and design of the thermal and elastic properties of the hexagonal lattice material: (a) Constituent solid material properties are a function of elemental composition and microstructure; (b) The mechanical properties of the underlying lattice structure are determined by the unit cell geometry of each layer (but thermal expansion is identical to that of the solid material); (c) The two types of lattice structure are combined to form a composite material with effective properties superior to those of the constituent phases.

Given the preceding assumptions and constitutive relations, the effective properties of the composite lattice material at the continuum level can be predicted from consideration of equilibrium and compatibility of deformation. The effective thermal expansion and effective elastic properties are given by

$$\overline{\alpha}_2 = \frac{H^A \epsilon_2^A + H^B \epsilon_2^B}{H^A + H^B} \frac{1}{\Delta T}, \tag{1}$$

and

$$\overline{C}_{ij} = \overline{C}_{ij}\left(C_{ij}^A, H^A, C_{ij}^B, H^B\right), \tag{2}$$

subject to equilibrium of forces,

$$\sigma_1^{\mathrm{A}} H^{\mathrm{A}} + \sigma_1^{\mathrm{B}} H^{\mathrm{B}} = 0, \quad \sigma_2^{\mathrm{A}} = \sigma_2^{\mathrm{B}} = 0, \tag{3}$$

and the compatibility condition

$$\epsilon_1^{\mathrm{A}} = \epsilon_1^{\mathrm{B}}. \tag{4}$$

The additional equilibrium and compatibility equations that are required derive from one of two assumptions about the boundary conditions of the material:

1. Plane stress boundary conditions: $\sigma_3^{\mathrm{A}} = \sigma_3^{\mathrm{B}} = 0$
2. Generalized plane strain boundary conditions: $\sigma_3^{\mathrm{A}} H^{\mathrm{A}} + \sigma_3^{\mathrm{B}} H^{\mathrm{B}} = 0, \quad \epsilon_3^{\mathrm{A}} = \epsilon_3^{\mathrm{B}}$.

Whether the material should be considered to be in a state of plane stress or a state of generalized plane strain depends on the thickness of the material in the 3-direction relative to the characteristic in-plane dimension of the hexagonal unit cell.

This analytical model can be used to predict the effective response of layered composites consisting of various combinations of solid materials, layer thicknesses, and unit cell geometries. As an example, we consider the following case:

- Aluminum and titanium constituent materials: $\dfrac{\alpha^{\mathrm{A}}}{\alpha^{\mathrm{B}}} = \dfrac{\alpha_{\mathrm{Al}}}{\alpha_{\mathrm{Ti}}} = \dfrac{23.6 \times 10^{-6}\,\mathrm{K}^{-1}}{8.6 \times 10^{-6}\,\mathrm{K}^{-1}} = 2.75$
- A single row of unit cells within each layer, with identical widths, $l^{\mathrm{A}}\cos\theta^{\mathrm{A}} = l^{\mathrm{B}}\cos\theta^{\mathrm{B}}$
- Unit cell aspect ratios $h^{\mathrm{A}}/l^{\mathrm{A}} = 1.5$, $h^{\mathrm{B}}/l^{\mathrm{B}} = 0.75$
- Cell wall aspect ratio $t^{\mathrm{A}}/l^{\mathrm{A}} = 0.1$ and cell wall thicknesses $t^{\mathrm{A}} = t^{\mathrm{B}}$
- Generalized plane strain boundary conditions

The model predicts that zero thermal expansion can be achieved with any permutation of the signs of the cell wall internal angles $(\pm\theta^{\mathrm{A}}, \pm\theta^{\mathrm{B}})$. However, θ^{B} can be varied much more widely when θ^{A} is negative than when θ^{A} is positive, demonstrating the importance of using an auxetic high CTE layer. Although the modeling results indicate that there are an infinite number of geometries that can exhibit zero thermal expansion, the thermal expansions in the 1-direction and the elastic moduli are different for most of these geometries. For the sets of cell wall internal angles at which the thermal expansion is zero, the CTE in the 1-direction, $\overline{\alpha}_1$, varies from $6.8 \times 10^{-6}\,\mathrm{K}^{-1}$ to $23.2 \times 10^{-6}\,\mathrm{K}^{-1}$ (Figure 6a). For these same cell wall internal angles, the elastic moduli each vary by over an order of magnitude: $\overline{E}_1 = 0.37 - 7.91$ GPa and $\overline{E}_2 = 0.093 - 1.36$ GPa (Figure 6b). Additionally, there are two sets of angles for which the material has the same elastic modulus in the 1-direction as it has in the 2-direction. The analytical modeling therefore demonstrates not

only the feasibility of controlling thermal expansion with this type of composite material but also the capability that the composite provides to tune material properties to the requirements of an application while still maintaining zero thermal expansion.

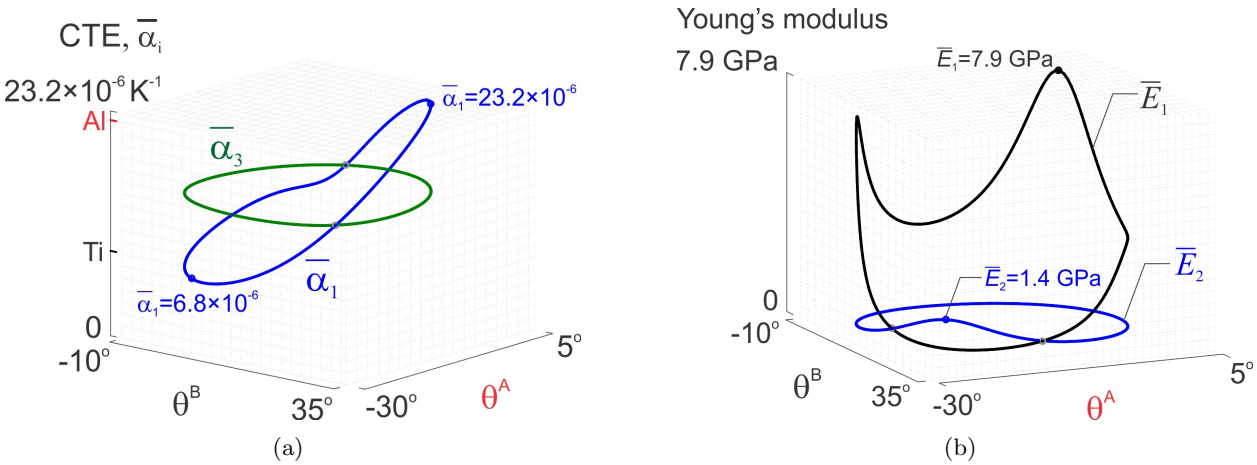

Figure 6. Predictions of analytical model for thermal and mechanical properties at zero transverse thermal expansion with $t^{\mathrm{A}}/l^{\mathrm{A}} = 0.1$: (a) Effective CTE in the 1-direction varies widely, but effective CTE in the 3-direction is nearly constant; (b) Young's modulus can be maximized in either direction or chosen to be the same in both directions.

3.1.2 Analytical modeling of composite triangular lattice structures

The mechanism for controlling thermal expansion in triangular lattice materials stems from the competition between rotation and expansion of structural elements. Referring back to Figure 4a, we consider one half of the triangular unit cell and approximate the nodes of the unit cell as pin joints because the elements have a much higher stiffness in axial loading than they have in bending. The change in height of the triangle is given by

$$(H + \delta H)^2 = (b + \delta b)^2 - \left(\frac{a + \delta a}{2}\right)^2, \tag{5}$$

in which $\delta a = \alpha^{\mathrm{A}} \Delta T$ and $\delta b = \alpha^{\mathrm{B}} \Delta T$. The effective thermal expansion in the 2-direction is simply

$$\overline{\alpha}_2 = \frac{\delta H}{H} \frac{1}{\Delta T}, \tag{6}$$

enabling us to write

$$\overline{\alpha}_2 = \frac{4\,(b/a)^2\,\alpha^{\mathrm{B}} - \alpha^{\mathrm{A}}}{4\,(b/a)^2 - 1}. \tag{7}$$

From the geometry of the unit cell, we also calculate the density of the structure or material:

$$\overline{\rho} = \frac{t}{H}\left(\frac{2b}{a}\rho^{\mathrm{B}} + \rho^{\mathrm{A}}\right), \tag{8}$$

where t is the cell wall thickness.

Plotting the predictions of the model in Figure 7, we see that zero thermal expansion can be attained even at modest ratios of constituent thermal expansion, such as $\alpha^{\mathrm{A}}/\alpha^{\mathrm{B}} = 1.5$. With a unit cell composed of aluminum and titanium elements ($\alpha^{\mathrm{A}}/\alpha^{\mathrm{B}} = 2.75$), zero thermal expansion occurs at a cell wall internal angle of 53°. This unit cell geometry is very close to the isotropic geometry ($\theta = 60°$) that achieves the Hashin-Shtrikman upper bound for isotropic materials, $\overline{E}/\overline{\rho} = 1/3 \times E_{\mathrm{s}}/\rho_{\mathrm{s}}$. At $\theta = 53°$, the density of the multimaterial structure is in the range of 300-900 kg/m^3 for typical cell wall thicknesses (Figure 7b). Dual material triangular structures can thus exhibit zero thermal expansion, excellent stiffness in both uniaxial and biaxial loading, and exceptionally low weight.

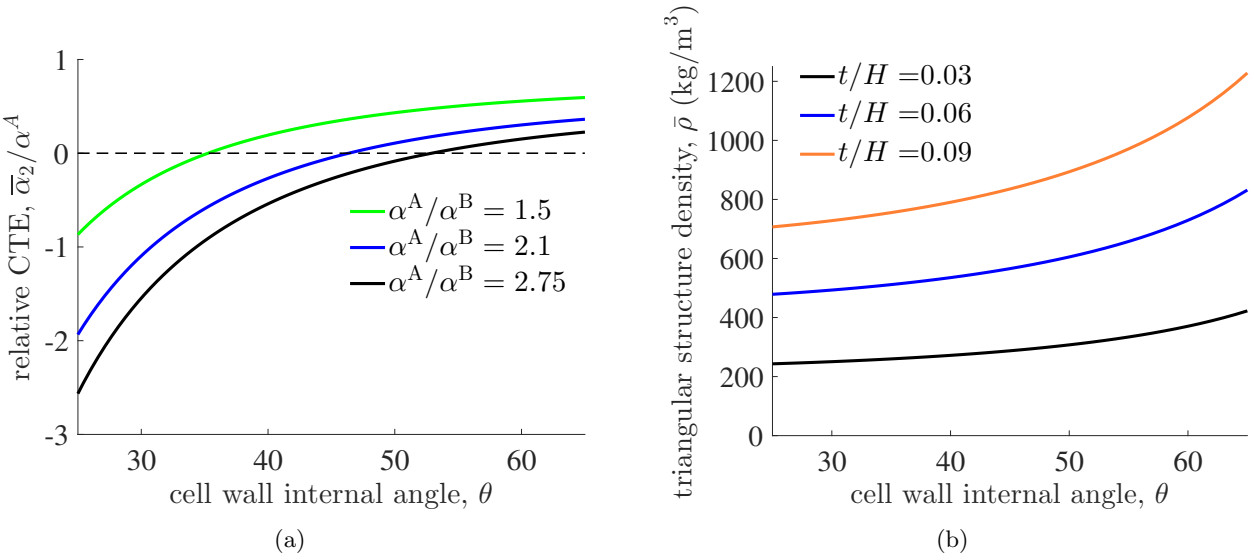

Figure 7. The properties of the triangular lattice structure can be tuned by changing its geometry: (a) Relative thermal expansion increases with increasing cell wall internal angle, θ; (b) Density increases with increasing cell wall aspect ratio and cell wall internal angle (calculated for $\rho_{\mathrm{Al}} = 2700$ kg/m^3, $\rho_{\mathrm{Ti}} = 4430$ kg/m^3*).*

3.1.3 Scaling relations for lattice materials

The properties and mechanical response of hexagonal and triangular lattice materials are well characterized by scaling relations. For isotropic, homogeneous materials (that is, $\theta_{\text{hex}} = 30^\circ$ and $\theta_{\text{tri}} = 60^\circ$), relative density increases linearly with increasing cell wall aspect ratio for both types of lattice (Gibson, 1997),

$$\frac{\overline{\rho}_{\text{hex}}}{\rho_{\text{s}}} = \frac{2}{\sqrt{3}}\left(\frac{t}{l}\right) \quad \text{and} \quad \frac{\overline{\rho}_{\text{tri}}}{\rho_{\text{s}}} = 2\sqrt{3}\left(\frac{t}{l}\right), \tag{9}$$

demonstrating the slight weight advantage of the hexagonal lattice for a given cell wall aspect ratio (Figure 8a). However, the stiffnesses of the two types of lattice scale very differently. With only three cell walls meeting at each joint ($Z = 3$), the deformation of hexagonal lattice-based materials is dominated by the bending of the cell walls, a compliant response that causes relative modulus, $\overline{E}/\overline{\rho_{\text{s}}}$, to scale with the cube of relative density:

$$\frac{\overline{E}_{\text{hex}}}{E_{\text{s}}} = \frac{3}{2}\left(\frac{\overline{\rho}_{\text{hex}}}{\rho_{\text{s}}}\right)^3. \tag{10}$$

On the other hand, triangular lattice-based materials have six cell walls meeting at each joint ($Z = 6$) and therefore exhibit a response dominated by stretching of the cell walls, a stiff, structurally efficient response that results in a linear relationship between modulus and relative density:

$$\frac{\overline{E}_{\text{tri}}}{E_{\text{s}}} = \frac{1}{3}\,\frac{\overline{\rho}_{\text{tri}}}{\rho_{\text{s}}}. \tag{11}$$

Plotted in Figure 8b, these scaling relations for stiffness illustrate the significant structural advantage of using triangular lattice-based materials to eliminate and control thermal expansion. For example, at a typical relative density of $\overline{\rho}/\rho_{\text{s}} = 0.15$, a triangular lattice material is nearly 10 times stiffer than a hexagonal lattice material is.

3.2 NUMERICAL MODELING OF COMPOSITE LATTICE MATERIALS

Micromechanical models of the hexagonal and triangular lattice materials were developed in order to simulate boundary conditions that are not periodic and to model the complex arrangement of constituent materials in the manufactured samples. A micromechanical model consists of four main components: (1) a representative volume element (RVE) that describes the geometry of a heterogeneous material; (2) boundary conditions that simulate the presence of adjoining material; (3) a model of the constitutive response of each material phase and interface; (4) a method to predict the macroscopic response of the heterogeneous material from the displacements and tractions at the boundaries of the RVE.

The underlying assumption of a micromechanical model is that the deformation of a heterogeneous material can be modeled at the continuum level by the deformation of a representative

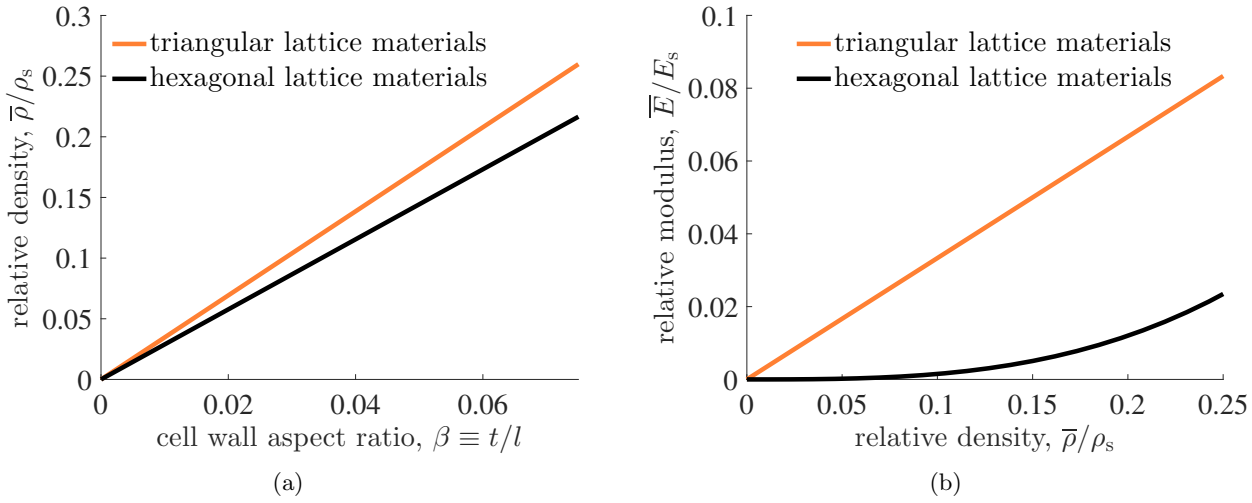

Figure 8. Scaling relations for hexagonal and triangular lattice-based materials demonstrate the superior structural efficiency of the triangular lattice: (a) For both types of material, relative density increases linearly with increasing cell wall aspect ratio, $\beta \equiv t/l$; (b) Conversely, the relative modulus of triangular lattice materials increases far more rapidly with increasing relative density than the modulus of hexagonal lattice materials does.

volume element of the material. An RVE is a section of the material that can be tessellated throughout space to generate the macro scale material. RVEs of the composite lattice materials consist of elements of both low CTE material and high CTE material (Figures 9 and 10). While, as shown in Section 3.1, these geometries and material configurations can be analyzed with analytical approaches, more complex cases require numerical methods. Here, we use the finite element method to model the deformation of the RVEs. Owing to symmetry, the finite element mesh needs to simulate only one half of the RVEs (Figures 9c and 10c). Compatibility of deformation requires the boundaries of the RVEs to remain straight for uniform loads or displacements applied parallel to the coordinate axes (no macroscopic shear). The constitutive response of each solid material phase is modeled as isotropic and linear elastic, and the cell walls are assumed to be perfectly bonded to each other at the interfaces between the two phases.

The macroscopic response of each RVE is calculated from the forces and displacements at the boundaries of the RVE. Continuity of the stresses requires that the average of the local Cauchy stress over the volume of the deformed RVE, $\mathbf{V}$, equals the macroscopically applied Cauchy stress:

$$\overline{\sigma}_1 = \frac{1}{V} \int_{\mathbf{x} \in \mathbf{V}} \sigma_1 (\mathbf{x}) \, \mathrm{d}V, \tag{12}$$

and

$$\overline{\sigma}_2 = \frac{1}{V} \int_{\mathbf{x} \in \mathbf{V}} \sigma_2 \left(\mathbf{x} \right) \mathrm{d}V, \tag{13}$$

which are evaluated by the equivalent surface integrals over the boundary of the RVE. The macroscopic logarithmic strains are calculated from the change in dimensions of the RVE:

$$\overline{\epsilon}_1 = \ln \left(W / W_0 \right), \tag{14}$$

and

$$\overline{\epsilon}_2 = \ln \left(H / H_0 \right), \tag{15}$$

where W and H are the width and height, respectively, of the RVE. In order to compute the effective thermal expansions of the RVE, a unit increase in temperature ΔT is imposed. The macroscopic displacement in each direction at the boundary, normalized by the original dimension, then provides the linear coefficient of thermal expansion of the RVE:

$$\overline{\alpha}_1 = \frac{u_1|_{X_1 = W_0}}{W_0} \quad \text{and} \quad \overline{\alpha}_2 = \frac{u_2|_{X_2 = H_0}}{H_0}, \tag{16}$$

where X_1 and X_2 are the coordinates in the undeformed configuration.

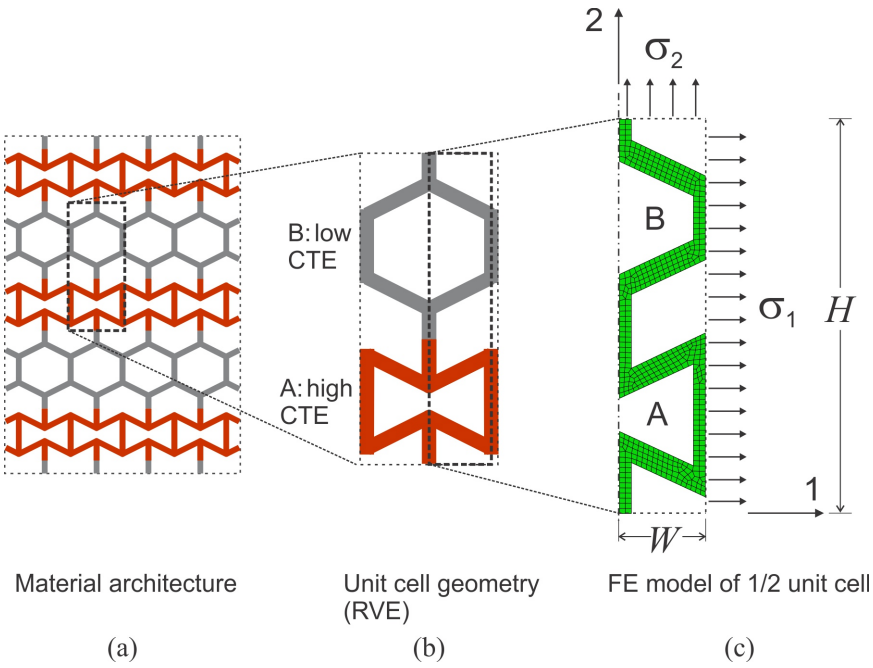

Figure 9. Numerical micromechanical modeling of a composite hexagonal lattice material: (a) Composite material at the macroscopic scale; (b) A representative volume element (RVE) of the composite material consists of one unit cell of each material; (c) Finite element model of the RVE simulating the effective response due to mechanical loading.

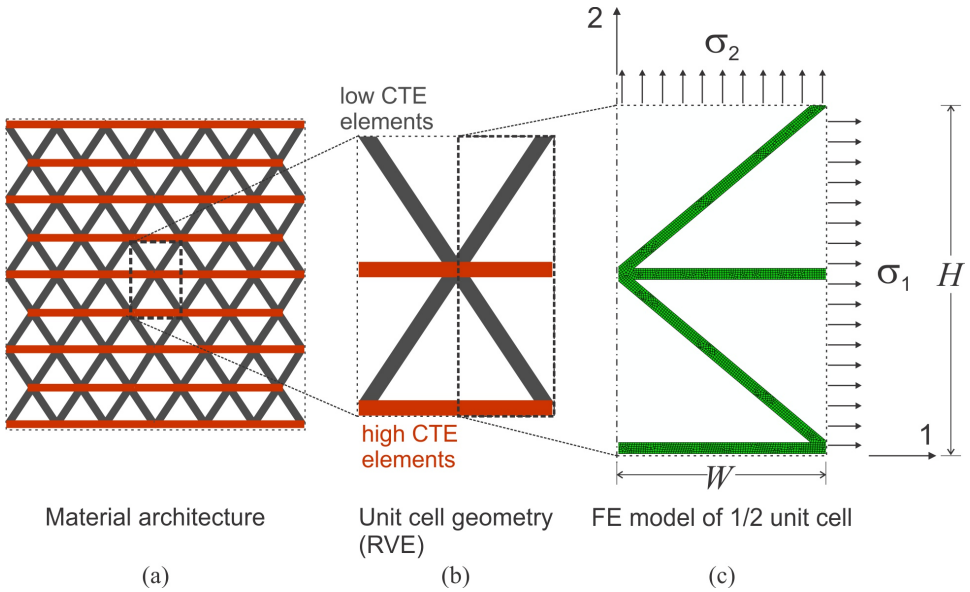

Figure 10. Numerical micromechanical modeling of a composite triangular lattice material: (a) Composite material at the macroscopic scale; (b) A representative volume element (RVE) of the composite material consists of a set of elements that form a unit cell; (c) Finite element model of the RVE simulating the effective response due to mechanical loading.

4. METHODS: SAMPLE MANUFACTURING AND TESTING

The models described in the previous section were used to design zero and negative thermal expansion materials that can be manufactured with automated methods at scales appropriate for aerospace, optomechanical, and device applications. Sample materials and structures were fabricated from aluminum and titanium with a recently developed 3D printing method, ultrasonic additive manufacturing (UAM), combined with post processing by computer-controlled electrical discharge machining. Following fabrication, the thermal expansion of the samples was measured optically with digital image correlation.

4.1 MANUFACTURING OF COMPOSITE LATTICE MATERIALS AND STRUCTURES BY 3D PRINTING AND ELECTRICAL DISCHARGE MACHINING

The first step in sample manufacturing was to print a composite plate from thin layers of aluminum and titanium in the desired layout. Although previously impossible to build, such a composite can now be readily printed at high resolution with ultrasonic additive manufacturing. UAM is a 3D printing process that builds metal composites from foils of dissimilar metals by ultrasonic welding. Because it uses foils as thin as 50 μm, the process is capable of producing small features. In UAM, a strip of foil 25.4 mm wide and up to about 200 μm thick is rolled out automatically over either a metal base plate or layers of previously consolidated foils. The foil is simultaneously pressed with a static normal force against the underlying metal layer (either the base plate or foils) by a rotating sonotrode. The sonotrode also oscillates at a high frequency (typically 20 kHz) in the direction transverse to the rolling direction. The frictional interaction between the newly deposited foil and the layer underneath breaks up surface oxides and contaminants and causes plastic deformation to occur, greatly improving surface contact. Local adiabatic heating promotes recrystallization of the deformed grains near the interface, and grain boundary motion across the interface results in the formation of dense metallurgical bonds between layers. Ultrasonic additive manufacturing can therefore robustly join many metals, including aluminum, titanium, copper, stainless steel, metal matrix composites, and combinations thereof (not to mention polymers).

An aluminum-titanium plate measuring 152 mm $\times$ 152 mm $\times$ 25.4 mm was 3D printed by Fabrisonic LLC of Columbus, OH (Figure 11a). The plate consisted of alternating layers of aluminum and nominally titanium, each 3.2 mm thick ($H^{\mathrm{A}} = H^{\mathrm{B}} = 3.2\,\mathrm{mm}$). The aluminum layers were composed of alternating foils of 6061 aluminum and 1100 aluminum, each 150 μm thick. The "titanium" layers were built from alternating foils of commercially pure Grade 2 titanium (150 μm thick) and 1100 aluminum (25 μm thick). The thin aluminum interlayer foils served as "glue" between the titanium foils because the high energy required to weld titanium to itself causes titanium also to weld to the steel sonotrode. (Fabricsonic is presently developing a ceramic sonotrode that should soon enable the welding of titanium foils directly to each another.)

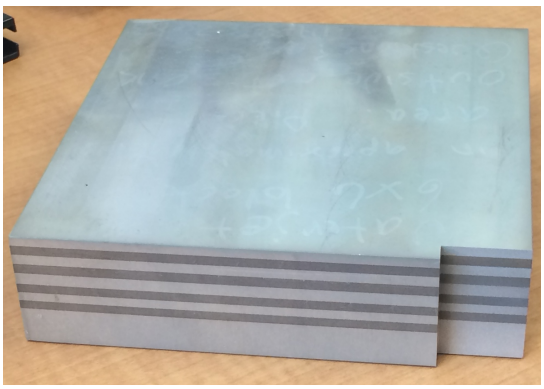

(a)

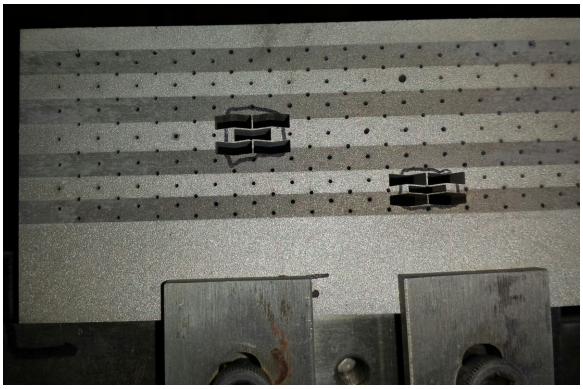

(b)

Figure 11. Hexagonal lattice materials and triangular lattice structures were manufactured with a combination of 3D printing and electrical discharge machining (EDM): (a) Eight alternating layers of titanium and aluminum, each 3.2 mm thick, were consolidated by ultrasonic additive manufacturing (UAM) to form the composite plate (total plate thickness is 38 mm, including the 12.7 mm aluminum baseplate); (b) During the EDM process, the holes for all the cells are first drilled, and then the wire is fed through the holes to cut out each hexagonal cell (shown) or triangular cell.

The post processing of the 3D printed composites was performed by electrical discharge machining (EDM) at Adron Tool Corp. in Menomonee Falls, WI. Samples 6.4 mm in thickness of various lengths were cut from the UAM composite plate, and the hexagonal or triangular cells were machined from the plate with computer numerical controlled EDM. During the EDM process, through-holes for all the cells were first drilled with a hole popper (Figure 11b). Then, a 0.008-inch wire was threaded through each hole to cut out the cell with wire EDM.

Two different designs of hexagonal lattice material were manufactured from the aluminum-titanium composite plate. In each of the samples, a single row of cells with a wall thickness of 200 μm was machined from each 3.2 mm thick layer of aluminum or titanium. The first sample was designed to have zero thermal expansion and consists of hexagonal cells machined from each layer (Figure 13a). This sample was successfully manufactured without any significant flaws. The second sample consists of solid aluminum layers at the top and bottom of height H^{solid} and a hexagonal lattice section at the center (Figures 12a and Figure 13b). The lattice section was designed to have a negative thermal expansion that counteracts the positive thermal expansion of the solid aluminum layers. As illustrated in Figure 14, the concept is to use this type of architecture as a building block for large, zero thermal expansion plates of size determined by the requirements of the application. The plates would be formed by joining sections with zero thermal expansion by methods such as vacuum brazing or ultrasonic soldering. The manufacturing of the second sample was also largely successful, but discontinuities in the cell walls were apparent at several locations,

caused by defects in the as-printed composite plate. The formation of defects would be prevented in future builds by performing a light stress relief after about every 10 mm of printing.

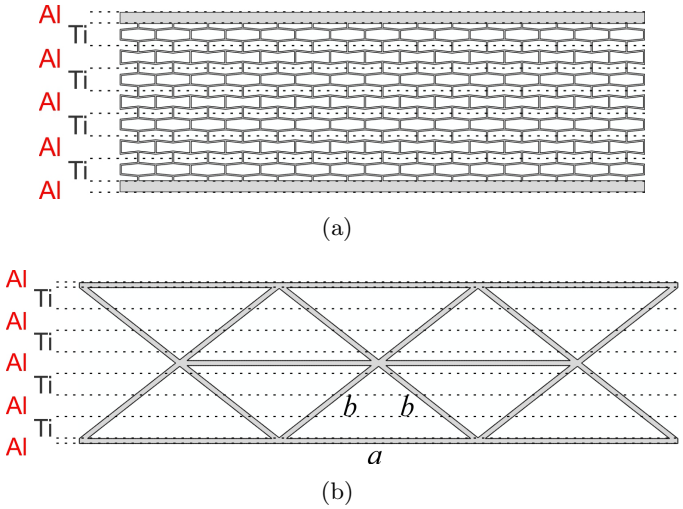

Figure 12. Schematics of geometry and arrangement of material in the dual material samples: (a) The hexagonal lattice material is composed of alternating cells of aluminum and titanium that are sandwiched top and bottom by solid aluminum layers; (b) The triangular lattice structures are composed of alternating layers of aluminum and titanium. The "a" elements (horizontal) are aluminum, and the "b" elements (diagonal) have a 3:2 ratio of titanium to aluminum.

Triangular lattice structures with cell wall internal angles $\theta = 26°,\ 40°,$ and $60°$ and cell wall thickness $t = 0.76$ mm were also manufactured from the aluminum-titanium plate (Figure 13c). In total, two rows of cells were machined in each sample, forming a fully triangulated truss with unit cell height $H = 12.2$ mm, as illustrated in Figure 12b. The horizontal a elements are aluminum and the diagonal b elements are predominantly titanium with a titanium volume fraction of about 60%, resulting in structural densities of $\overline{\rho} = 420$-620 kg/m^3. It is envisioned that such triangular lattice structures with zero thermal expansion could be joined to form large plates of virtually any size (Figure 15).

4.2 MEASUREMENT OF THERMAL EXPANSION OF COMPOSITE LATTICE MATERIALS AND STRUCTURES

The coefficient of thermal expansion of each sample was measured with digital image correlation and a custom-built temperature chamber and image acquisition system. While the sample was heated, images of the sample were acquired at regular intervals and the temperature of the sample

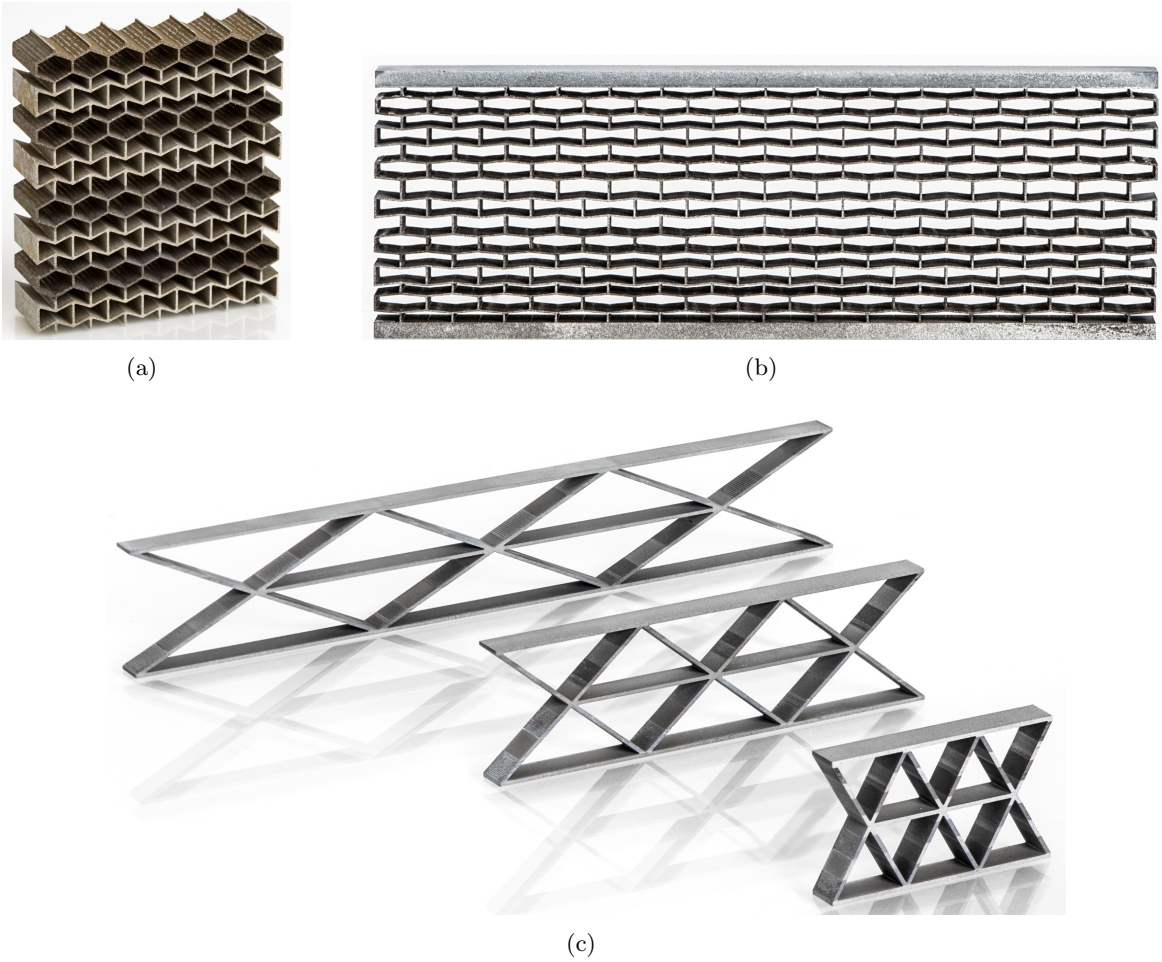

(a) (b)

(c)

Figure 13. Composite lattice materials and structures for controlling thermal expansion (all measuring about 25.4 mm tall): (a) Hexagonal lattice material designed for zero thermal expansion and maximum specific stiffness in bending; (b) Hexagonal lattice material designed for minimum thermal expansion (i.e., negative) and with solid top and bottom layers so that sections can be joined to form large plates; (c) Triangular lattice structures, with cell wall internal angle and CTE increasing from left to right.

was simultaneously recorded. After the heating process, the coefficient of thermal expansion was calculated by performing digital image correlation on each image.

The experimental apparatus consisted of a temperature chamber, an optical system, and the electronics for the measurement of temperature (Figure 16). The sample was placed on an aluminum hot plate (Wenesco HP99URS-JHQ) and surrounded by a 1.5 inch thick frame of calcium silicate insulation. A 0.25 inch thick sheet of borosilicate glass was placed on top of the insulation to

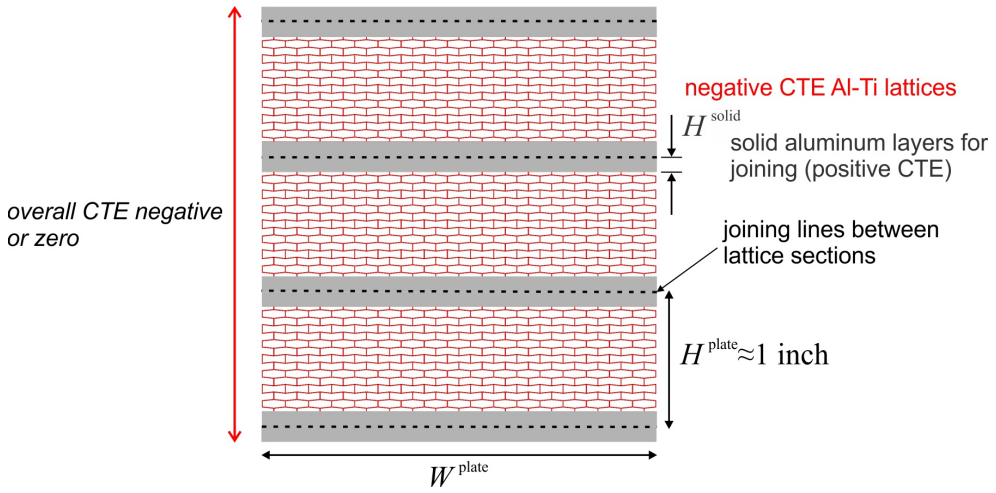

Figure 14. Large plates with zero thermal expansion can be manufactured by joining short sections with negative CTE. Solid aluminum layers enable joining, and the negative CTE of the Al-Ti lattice sections compensates for the positive CTE of the solid aluminum layers.

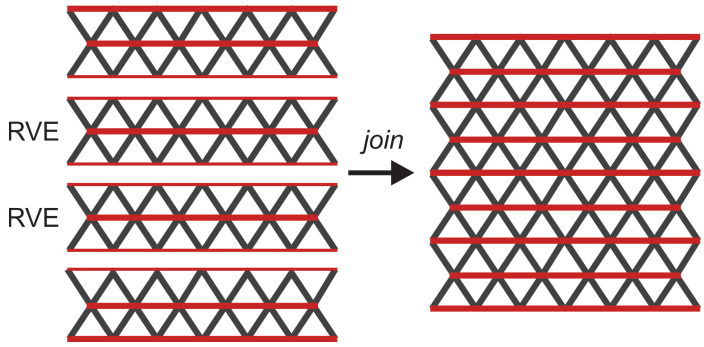

Figure 15. Large plates with zero thermal expansion can be manufactured by joining short triangular trusses, each exhibiting zero CTE.

seal the chamber and reduce the heating of the air between the sample and the camera. The hot plate rested on a honeycomb optical breadboard (Newport Nexus). Suspended by optical posts, a high resolution CMOS cameras (FLIR Grasshopper3) was mounted above the sample to a two-axis linear translation stage used to position and focus the optics. Depending on the size of the sample and the desired image magnification, a working distance of either 22.2 cm or 50.8 cm and either a 55 mm f/2.8 or a 105 mm f/2.8 SLR lens were used. During the tests, the samples were illuminated by two LED light sources (Thorlabs and Schott KL 2500), and the temperature was measured with a minimum of two Type J thermocouples (OMEGA 5TC-GG-J-30-72). The output voltage of

the thermocouples was acquired with a National Instruments NI-9211 Temperature Input Module mounted in a CompactDAQ chassis. Starting at room temperature, the sample was heated at a rate of 2 °C/min to a maximum of 150 °C, and images were captured at intervals of 10 s. A fan was used to mix the air above the sample so that image distortion caused by convective currents was minimized.

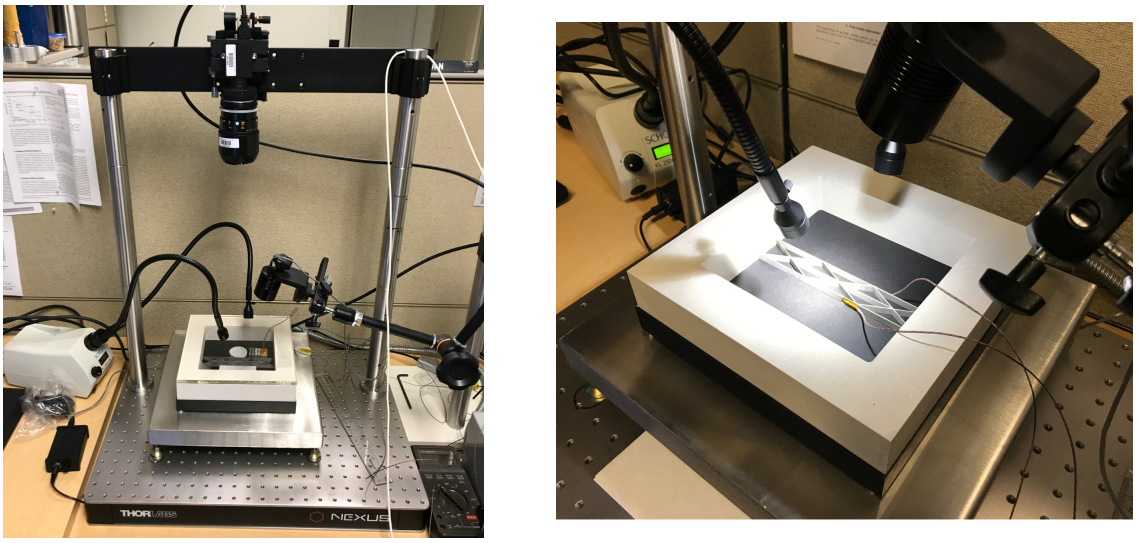

(a) (b)

Figure 16. The thermal expansion of the samples was measured optically with digital image correlation: (a) Apparatus for acquiring images of the specimen as it is heated on a hot plate; (b) Close-up of the hot plate, temperature chamber, LED lighting, and specimen instrumented with thermocouples (glass plate sealing the chamber not in place).

After the tests were completed, the images were post processed with digital image correlation software (Correlated Solutions, Irmo, SC). In digital image correlation, square subsets of pixel gray level values ($\sim 50\,\text{px} \times 50\,\text{px}$) are mapped from a reference image to each deformed image, enabling calculation of the displacement of the center of each subset with high accuracy. The displacement calculation is repeated at many overlapping subsets, and strains are then computed from averaged values of displacement. The resolution of digital image correlation is often improved by applying a speckle pattern to the sample, but, with our lattice material samples, the surface texture alone provided sufficient variation of pixel gray level values.

A complication associated with the use of digital image correlation is error caused by out-of-plane motion. If the sample or fixturing moves or changes dimension in the direction of the optical axis, then 2D digital image correlation will measure this motion as an in-plane displacement. For

an out-of-plane translation ΔZ, defined to be positive when the sample moves toward the lens and camera, the apparent displacement field in the coordinate frame of the image sensor is approximately

$$u_{\mathrm{s}} = x_{\mathrm{s}} \frac{\Delta Z}{Z}, \quad \text{and} \quad v_{\mathrm{s}} = y_{\mathrm{s}} \frac{\Delta Z}{Z}, \tag{17}$$

where Z is the object distance ($\approx$ working distance) and $(x_{\mathrm{s}}, y_{\mathrm{s}})$ is the position of a point in the sensor plane. The resulting fictitious strain field due to the out-of-plane motion is

$$\epsilon_{\mathrm{xx}} = \frac{\partial u_{\mathrm{s}}}{\partial x_{\mathrm{s}}} = \frac{\Delta Z}{Z}, \quad \text{and} \quad \epsilon_{\mathrm{yy}} = \frac{\partial v_{\mathrm{s}}}{\partial y_{\mathrm{s}}} = \frac{\Delta Z}{Z}. \tag{18}$$

In summary, when the sample translates or expands toward the camera, digital image correlation registers this motion as a non-physical in-plane expansion. In order to minimize error caused by out-of-plane motion, the object distance should be as large as possible.

There were two sources of out-of-plane motion during the testing of the lattice materials: (1) the thermal expansion of the sample in the 3-direction, $\overline{\alpha}_3$; (2) the thermal expansion of the aluminum hot plate. The error caused by the thermal expansion of the sample is

$$\overline{\alpha}_{\mathrm{error}} \approx \frac{\overline{\alpha}_3 \, t^{\mathrm{plate}}}{Z}, \tag{19}$$

where t^{plate} is the thickness of the sample. This error was minimized by specifying the working distance to be least 22 cm for all tests (and over 50 cm in most cases). $\overline{\alpha}_{\mathrm{error}}$ is calculated to be less than $0.5 \times 10^{-6}\,\mathrm{K}^{-1}$, even at the shortest working distance, and was therefore determined to be negligible. On the other hand, the thermal expansion of the aluminum hot plate itself can be significant and was accounted for by calibrating the set-up at each working distance.

The error in the measurement of thermal expansion caused by the motion of the hot plate was determined by measuring the apparent expansion of aluminum 6061 and fused silica, two materials with well known CTEs ($\alpha_{\mathrm{Al}} = 23.6 \times 10^{-6}\,\mathrm{K}^{-1}$ and $\alpha_{\mathrm{fs}} = 0.55 \times 10^{-6}\,\mathrm{K}^{-1}$, respectively). In the initial set-up, the working distance was 22.2 cm, and a 5 megapixel camera and only one light source were used. At this working distance, the apparent thermal expansion of a 1.6 mm thick aluminum 6061 plate was measured to be $35.5 \times 10^{-6}\,\mathrm{K}^{-1}$, resulting in an apparent fixture expansion of $\alpha_{\mathrm{fixture1}} = 11.9 \times 10^{-6}\,\mathrm{K}^{-1}$ (Figure 17). In the second set-up, used for the majority of the tests, the working distance was 52 cm, and a 12.3 megapixel camera and two light sources were used. The increase in working distance, sensor size, and light intensity significantly improved the accuracy and resolution of the measurements. In this case, the apparent thermal expansion of a 3.2 mm sample of fused silica was measured to be $5.62 \times 10^{-6}\,\mathrm{K}^{-1}$ (Figure 18). From this measurement, the apparent thermal expansion caused by the motion of the hot plate is calculated to be $\alpha_{\mathrm{fixture2}} = 5.06 \times 10^{-6}\,\mathrm{K}^{-1}$. In order to verify the calibration, the apparent thermal expansion of a 3.2 mm thick aluminum 6061 plate was then measured. Subtracting the calibration factor, $\alpha_{\mathrm{fixture2}}$, the actual thermal expansion of the aluminum plate sample is calculated to be $\alpha_{\mathrm{Al-measured}} = 23.7 \times 10^{-6}\,\mathrm{K}^{-1}$, agreeing with the known value and therefore confirming the accuracy of the method of measuring thermal expansion.

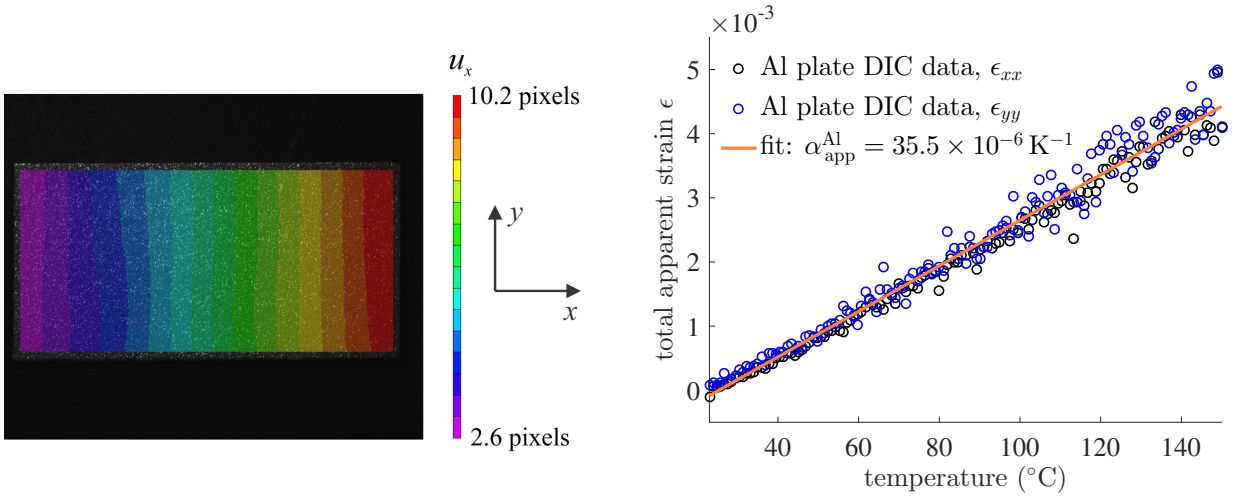

Figure 17. Initial set-up (22.2 cm working distance) was calibrated by measuring the apparent thermal expansion of an aluminum plate (known $\alpha_{\text{Al}} \equiv 23.6 \times 10^{-6}\,\text{K}^{-1}$*) with digital image correlation (DIC): (a) Full-field displacements measured by DIC in the x-direction caused by heating to* $T = 150\,^{\circ}\text{C}$*; (b) Apparent expansion measured* $\alpha_{\text{app}} = 35.5 \times 10^{-6}\,\text{K}^{-1}$*, resulting in an out-of-plane error caused by the expansion of the hot plate of* $\alpha_{\text{fixture1}} = 35.5 \times 10^{-6}\,\text{K}^{-1} - \alpha_{\text{Al}} = 11.9 \times 10^{-6}\ \text{K}^{-1}$.

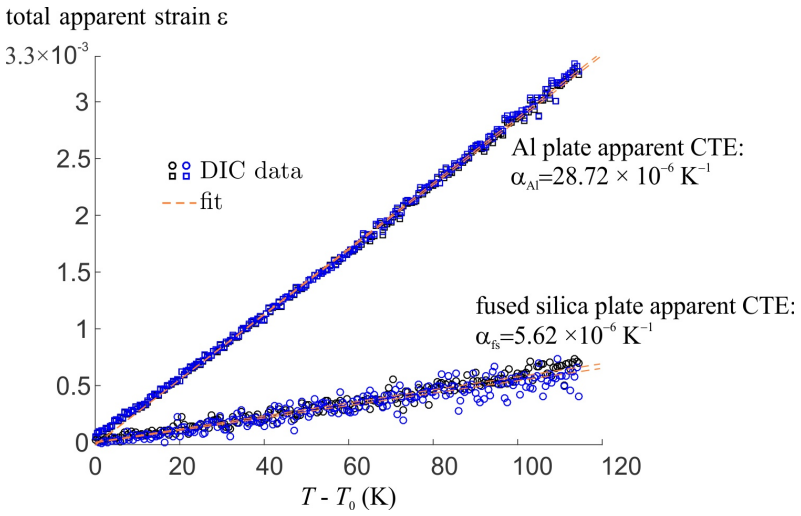

Figure 18. Second set-up (52 cm working distance) was calibrated by measuring the apparent thermal expansion of fused silica (known $\alpha_{\mathrm{fs}} \equiv 0.55 \times 10^{-6}\,\mathrm{K}^{-1}$*), resulting in an out-of-plane error caused by the expansion of the hot plate* $\alpha_{\mathrm{fixture2}} = 5.62 \times 10^{-6}\,\mathrm{K}^{-1} - \alpha_{\mathrm{fs}} = 5.06 \times 10^{-6}\,\mathrm{K}^{-1}$*. Therefore, the measured thermal expansion of the aluminum plate was* $\alpha_{\mathrm{Al-measured}} = 28.72 \times 10^{-6}\,\mathrm{K}^{-1} - \alpha_{\mathrm{fs}} = 23.7 \times 10^{-6}\,\mathrm{K}^{-1}$*, verifying the accuracy of the method of measuring CTE.*

This page intentionally left blank.

5. RESULTS: MODEL PREDICTIONS, MATERIAL DESIGNS, AND EXPERIMENTAL VALIDATION

In this section, modeling predictions and experimental results are presented for both types of zero thermal expansion material. Simulation results are compared with measurements, and the results of additional simulations are used to explore further the mechanics involved in controlling thermal expansion with composite lattice materials.

5.1 MODELING AND DESIGN OF COMPOSITE HEXAGONAL LATTICE MATERIALS

We implemented the analytical model of Section 3.1.1 into an optimization algorithm in order to design a prototype zero CTE hexagonal material. Although there are still many hexagonal geometries that exhibit zero CTE, the thicknesses of the layers in the 3D printed composite plate impose an additional constraint upon the hexagonal material design:

$$H^{\mathrm{A}} = H^{\mathrm{B}} \equiv H^{\mathrm{cell}}. \tag{20}$$

Subject to this constraint and also taking the cell wall thicknesses to be $t^{\mathrm{A}} = t^{\mathrm{B}} \equiv t$ to facilitate manufacturing, the geometry of the zero CTE hexagonal material was designed to maximize the material performance index for the bending of a plate or panel:

$$M^{\mathrm{plate}} = \frac{(\overline{E}_2)^{\frac{1}{3}}}{\overline{\rho}}. \tag{21}$$

M^{plate} should be maximized to build the lightest panel or plate for a specified bending stiffness or to maximize flexural vibration frequency for a specified stiffness or mass. (In these cases, respectively, mass and flexural vibration frequency would scale inversely with M^{plate}.) For all results presented in Section 5, the materials are modeled as linear elastic with $E^{\mathrm{A}} = 68.9\,\mathrm{GPa}$, $\nu^{\mathrm{A}} = 0.33$, $\alpha^{\mathrm{A}} = 23.6 \times 10^{-6}\,\mathrm{K}^{-1}$ and $E^{\mathrm{B}} = 105.9\,\mathrm{GPa}$, $\nu^{\mathrm{A}} = 0.37$, $\alpha^{\mathrm{A}} = 8.6 \times 10^{-6}\,\mathrm{K}^{-1}$, representing aluminum and titanium, respectively.

The results of the optimization procedure show that a composite hexagonal lattice material can be manufactured with both zero CTE and mechanical properties superior to the properties of aluminum and Invar. The material performance index increases with decreasing cell wall aspect ratio t/H^{cell} but is not particularly sensitive to the unit cell aspect ratio, $h^{\mathrm{A}}/l^{\mathrm{A}}$ (Figure 19a). At each t/H^{cell}, the material performance index is maximum at $h^{\mathrm{A}}/l^{\mathrm{A}} \approx 1.5$. As the cell walls become thinner, the material performance index increases from about equal to the index of aluminum and twice the index of Invar to almost four times the index of aluminum and nearly ten times the index of Invar. Over this range of cell wall aspect ratios, the density of the lattice material decreases from about 930 $\mathrm{kg/m^3}$ to 110 $\mathrm{kg/m^3}$ (Figure 19b).

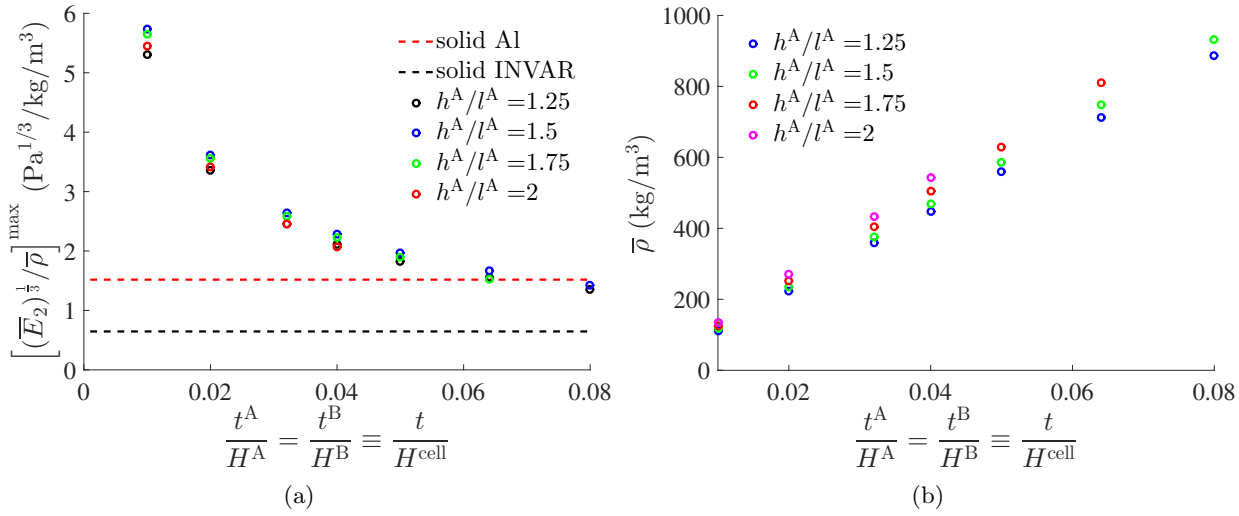

Figure 19. Optimizing the geometry of the hexagonal lattice material to achieve zero thermal expansion and maximize the material performance index for the bending of a plate or panel, M^{plate} (generalized plane strain case): (a) M^{plate} of the optimized hexagonal lattice material is superior to the indices of solid aluminum and solid Invar at most cell wall aspect ratios; (b) The densities of the optimized hexagonal lattice material are all much lower than the densities of solid aluminum and solid Invar.

The cell wall internal angles that result in zero CTE and maximum specific stiffness vary as the cell wall aspect ratios change. As the cell wall aspect ratios decrease from $t/H^{cell} = 0.08$ to $t/H^{cell} = 0.01$, the cell wall internal angles range from ($\theta^A = -22.3°$, $\theta^B = 24.3°$) to ($\theta^A = -27.6°$, $\theta^B = 27.9°$) for the case of generalized plane strain and ($\theta^A = -26.9°$, $\theta^B = 28.6°$) to ($\theta^A = -29.9°$, $\theta^B = 30.0°$) for the case of plane stress. Based on these predictions and assuming generalized plane strain deformation, we designed and manufactured a sample with zero CTE and maximized specific stiffness with $t/H^{cell} = 0.064$, $h^A/l^A = 1.33$, $\theta^A = -22.8°$, and $\theta^A = 24.0°$ (Figure 13a). This particular geometry results in a density of about $\overline{\rho} = 710\,\text{kg/m}^3$. The measurement of the thermal expansion of this sample is presented below in Section 5.3.

In addition to the analytical study just described, we conducted parametric studies of the effect on effective thermal expansion of the sample width, W^{plate}, the sample thickness, t^{plate}, and the thin aluminum interlayers within the otherwise titanium layers. The dimensions of the sample impact its thermal expansion only when the width or thickness is not significantly larger than the size of each hexagonal cell. These effects cannot be captured by analytical models because the boundary conditions are not periodic. Numerical models of finite sized samples and RVEs were therefore constructed for this purpose.

The effect on overall thermal expansion of sample thickness, t^{plate}, was investigated by comparing the results of 3D finite element (FE) simulations with the results of 2D simulations conducted with plane stress and generalized plane strain boundary conditions. The in-plane geometry of the hexagonal cells was held constant at the geometry predicted by the analytical modeling to result in zero CTE with maximum specific stiffness in generalized plane strain ($t/H^{\text{cell}} = 0.064$, $h^{\text{A}}/l^{\text{A}} = 1.5$, $\theta^{\text{A}} = -24.6°$, and $\theta^{\text{A}} = 25.9°$). With the same geometry and boundary conditions, a 2D numerical simulation of the RVE predicts an effective CTE, $\overline{\alpha}_2$, of less than $2.5 \times 10^{-7}\,\text{K}^{-1}$, negligibly small and thus validating the predictions of the analytical model. With plane stress boundary conditions, however, the 2D simulation predicts a significantly larger CTE of $\overline{\alpha}_2 = 4.0 \times 10^{-6}\,\text{K}^{-1}$ because each layer is free to expand in the 3-direction, reducing the constraint stresses in the 1-direction. In order to investigate the relationship between the thickness of the sample and the effective thermal expansion, 3D solid models of the zero CTE, maximum specific stiffness sample were constructed with various thicknesses. Figure 20 shows the solid model of the manufactured test sample, which has a thickness ratio $t^{\text{plate}}/H^{\text{cell}} = 2$ (i.e., $t^{\text{plate}} = 6.4$ mm). The results of the 3D simulations show that is not until $t^{\text{plate}}/H^{\text{cell}} \approx 10$ that the sample approaches the generalized plane strain condition (Figure 21a). In fact, at $t^{\text{plate}}/H^{\text{cell}} = 2$, the sample is closer to a plane stress condition than it is to a generalized plane strain condition.

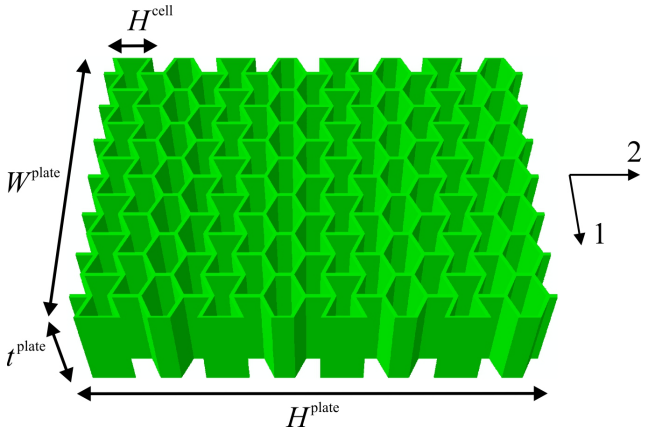

Figure 20. Parametric 3D finite element simulations of the hexagonal lattice material were performed in order to investigate the effect on thermal expansion of plate thickness, t^{plate}. (Shown is the solid model of the hexagonal lattice material designed for zero CTE and maximum specific stiffness in bending.)

In further simulations of this type, the thin aluminum interlayers were added between the titanium foils in the B layers. The introduction of high CTE material into the low CTE layers decreases the contrast in CTE between the A layers and the B layers and thus reduces the Poisson effect that causes zero thermal expansion. As shown in Figure 21b, the effective thermal expansion

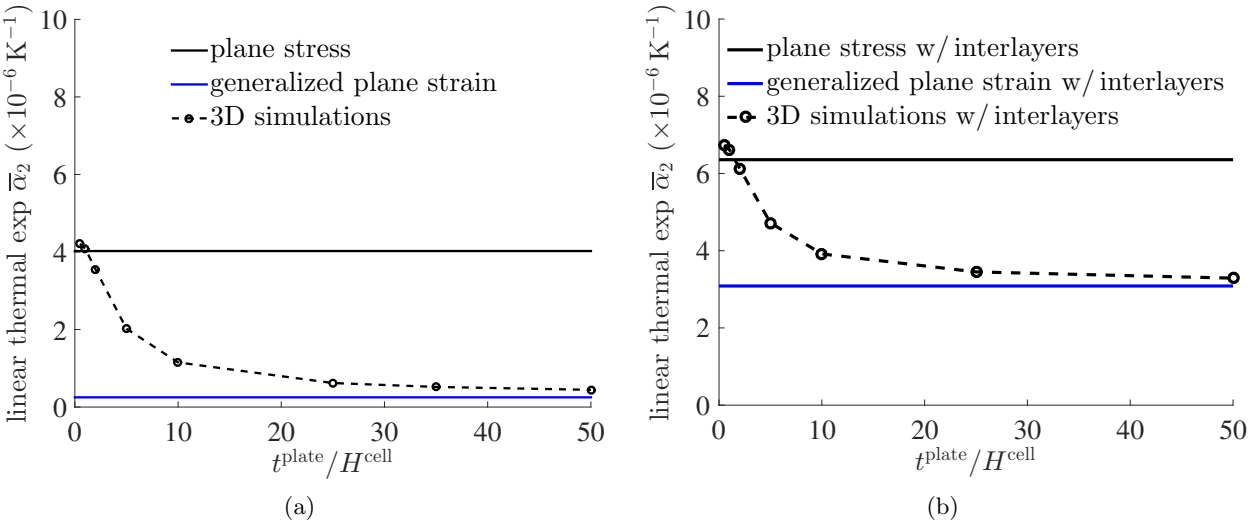

Figure 21. The finite thickness of the plate, t^{plate}, and the presence of the thin aluminum interlayers within the nominally titanium layers (B layers) both increase the effective thermal expansion of the hexagonal lattice material, $\overline{\alpha}_2$; (a) As the thickness of the plate increases, $\overline{\alpha}_2$ approaches zero as the response transitions from plane stress to generalized plane strain ($\epsilon_3^{\mathrm{A}} = \epsilon_3^{\mathrm{B}}$); (b) The aluminum interlayers increase $\overline{\alpha}_2$ by 2-3 $\times\, 10^{-6}\,\mathrm{K}^{-1}$.

of the sample therefore increases by 2-3 $\times\, 10^{-6}\,\mathrm{K}^{-1}$ in all the simulations. (The effect of the aluminum interlayers was not included in the analytical model.)

In a second parametric study, the effect on overall thermal expansion of the width of the sample, W^{plate}, was investigated with numerical simulations. At the free surfaces of the sample normal to the 1-direction, all components of the traction vector are zero, and no Poisson contraction occurs due to expansion in the 1-direction. Performing simulations under conditions of generalized plane strain at different sample aspect ratios, $W^{\mathrm{plate}}/H^{\mathrm{cell}}$, we show that the width of the sample must reach $W^{\mathrm{plate}}/H^{\mathrm{cell}} \approx 25$ before the effect of the free surfaces becomes negligible (Figure 22).

We also developed the capability to predict the unit cell geometries that cause minimum thermal expansion, including negative CTE. Negative CTE lattice materials can be combined with positive CTE materials to build materials or systems with zero overall CTE (Figure 14). Figure 23a shows the predictions of the analytical model for the effective thermal expansion as a function of θ^{A} and θ^{B} (plane stress conditions, $t/H^{\mathrm{cell}} = 0.064$, $h^{\mathrm{A}}/l^{\mathrm{A}} = 0.75$, subject to the constraints of the UAM composite plate). The function exhibits a single minimum point, without any local minima, and is therefore well suited for minimization by numerical methods. We use the downhill simplex method to determine the combination of cell wall internal angles that produces minimum thermal expansion (Press, 2007). Two minimization algorithms were developed, each with a different

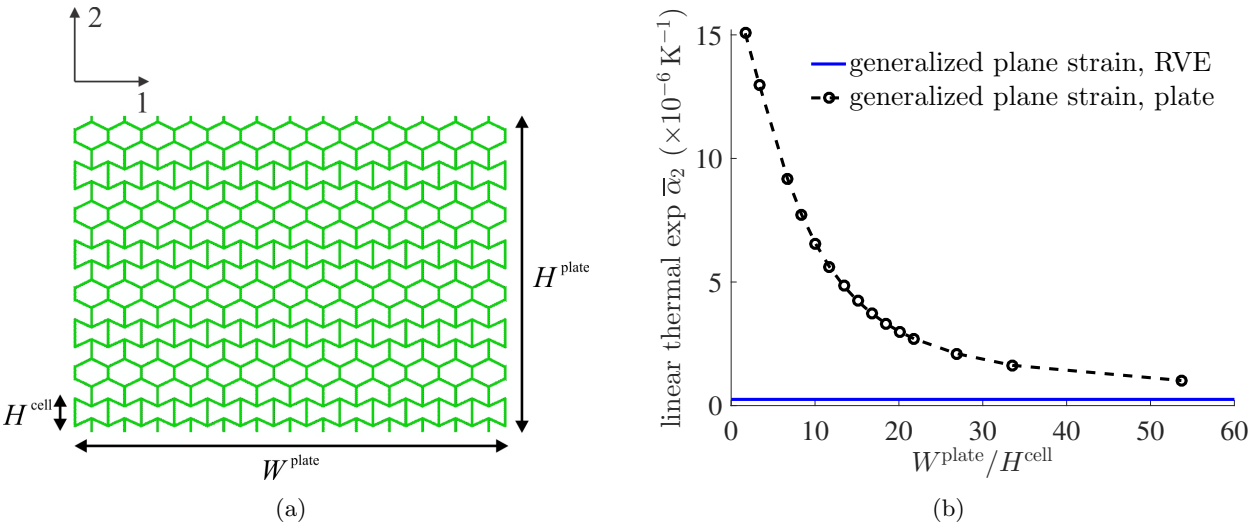

Figure 22. The finite width of the plate increases the effective thermal expansion of the hexagonal lattice material, $\overline{\alpha}_2$: (a) Solid model of the plate with $W^{\text{plate}}/H^{\text{cell}} = 10$; (b) As the width of the plate increases, $\overline{\alpha}_2$ approaches zero as the response transitions from the structural response to the RVE response (which has periodic boundary conditions, by definition).

method of calculating the thermal expansion at the evaluation points of the simplexes. One method uses the analytical model, and the other uses a micromechanical FE simulation. These algorithms were used to predict the cell wall internal angles that minimize the thermal expansion of a lattice material consisting of three A layers of aluminum and four B layers of titanium (Figure 14). The analytical and numerical algorithms produce almost identical results, but the numerical algorithm enables straightforward inclusion of the aluminum interlayers within the B layers. Considering the effect of these interlayers in the model and minimization algorithm, the minimum CTE for the plane stress case with $t/H^{\text{cell}} = 0.064$ and $h^{\text{A}}/l^{\text{A}} = 0.75$ was predicted to be $\overline{\alpha}_2 = 41.8 \times 10^{-6}\,\text{K}^{-1}$ at $\theta^{\text{A}} = -7.2°$ and $\theta^{\text{B}} = 7.1°$ (Figure 23b). A sample with this RVE geometry, a thickness of $t^{\text{plate}} = 6.4\,\text{mm}$, and a width of $W^{\text{plate}} = 77.4$ mm was manufactured from the UAM composite plate (Figure 13b).

In the formation of large samples or structures from sections of negative CTE material joined with sections of positive CTE material, the effect on overall thermal expansion of the positive CTE sections must also be considered. In Section 4.1 and Figure 14, we introduced a concept material in which negative CTE lattice material is separated by solid layers of aluminum with height H^{solid}. Numerical simulations of each plate section show that the effective thermal expansion of the plate increases with increasing H^{solid} because the layers with positive CTE comprise an increasing volume fraction of the section (Figure 24a). The simulations also indicate that the effective thermal

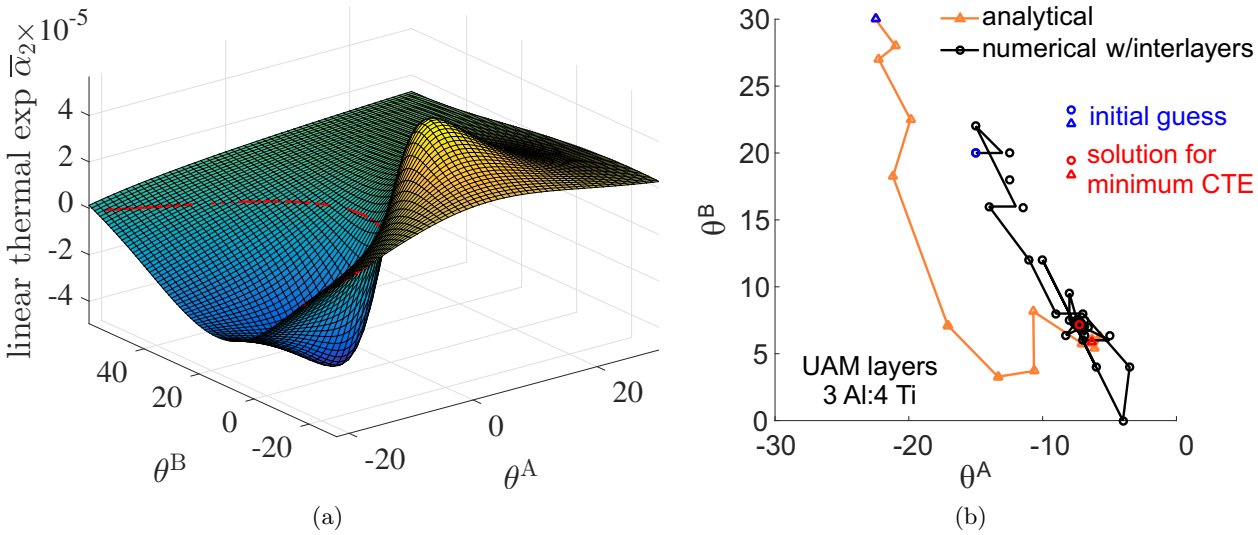

Figure 23. Designing a hexagonal lattice material with negative effective thermal expansion for combination with materials with positive thermal expansion: (a) Many combinations of cell wall internal angles produce zero or negative thermal expansion (analytical modeling results for plane stress with $t/H^{\text{cell}} = 0.064$ and $h^{\text{A}}/l^{\text{A}} = 0.75$); (b) The cell wall internal angles $(\theta^{\text{A}}_{\text{min}}, \theta^{\text{B}}_{\text{min}})$ that minimize thermal expansion in this case are determined numerically by the downhill simplex method, with the effective thermal expansion calculated either with the analytical model or by the finite element method (for the case with the aluminum interlayers within the B layers).

expansion decreases with increasing plate aspect ratio, $W^{\text{plate}}/H^{\text{plate}}$, caused by the decreasing significance of the effect of the free surfaces, as discussed above. Additional simulations show that the effective thermal expansion of the plate section with finite dimensions asymptotes to the response of the unit cell and the section RVE at $W^{\text{plate}}/H^{\text{plate}} \approx 5$ (Figure 24b). The response of the section RVE models the deformation of a plate that is infinite in height but finite in width. In a plate composed of many individual sections, symmetry requires the top and bottom of all interior sections to remain flat, identical to the response of the section RVE. Otherwise, the deformation would not satisfy the geometric compatibility conditions.

5.2 MODELING AND DESIGN OF COMPOSITE TRIANGULAR LATTICE STRUCTURES

As described in Section 4.1, samples of the triangular lattice structures were manufactured from the UAM composite plate (Figures 12b and 13c). In these samples, the diagonal "b" elements were themselves composed of multiple materials, with the majority of each element consisting of titanium. Because the arrangement of material within the diagonal elements was complex, the

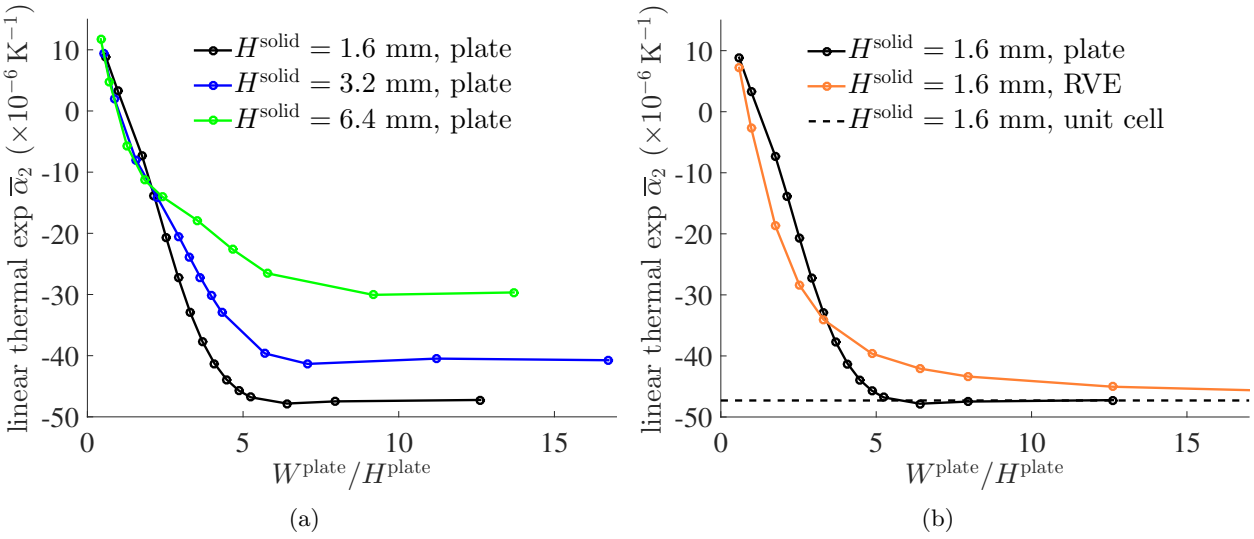

Figure 24. Design of a hexagonal lattice material with solid top and bottom aluminum layers that enable joining of short sections to form large plates with zero or negative effective thermal expansion (with cell wall internal angles fixed at $\theta^{\mathrm{A}}_{\mathrm{min}}, \theta^{\mathrm{B}}_{\mathrm{min}}$): (a) Increasing the thickness of the solid aluminum layers decreases the thermal expansion of the material; (b) The thermal expansion approaches the unit cell response and RVE response ($u_2 = \mathrm{constant}$) at a plate aspect ratio of $W^{\mathrm{plate}}/H^{\mathrm{plate}} \approx 10$. (All simulations were conducted with plane stress boundary conditions.)

thermal expansion of these structures were simulated numerically with the finite element method. A state of plane stress was assumed because, at 6.4 mm, the thickness of the samples was only twice the thickness of each A (aluminum) and B (titanium) layer. In the constitutive relations, the titanium layers containing the thin aluminum interlayers were modeled at the continuum level as transversely isotropic sections with elastic constants $E^{\mathrm{B}}_1 = 99.8\,\mathrm{GPa}$, $E^{\mathrm{B}}_2 = 97.7\,\mathrm{GPa}$, $\nu^{\mathrm{B}}_{12} = 0.364$, and $G^{\mathrm{B}}_{12} = 35.9\,\mathrm{GPa}$, calculated from the effective medium theories of Voigt and Reuss. The effective thermal expansions were calculated from the equilibrium and compatibility equations that describe free thermal expansion under conditions of plane stress as $\alpha^{\mathrm{B}}_1 = 10.0 \times 10^{-6}\,\mathrm{K}^{-1}$ and $\alpha^{\mathrm{B}}_2 = 11.2 \times 10^{-6}\,\mathrm{K}^{-1}$. Simulations were conducted with various cell wall internal angles, θ. (Figure 12b shows the solid model of the triangular structure with $\theta = 26\,^\circ$.) The predictions of the simulations are presented together with the experimental results in the following section.

5.3 EXPERIMENTAL RESULTS AND COMPARISON WITH MODEL PREDICTIONS

Here, in the conclusion of the results section, the measurements of thermal expansion and the predictions of numerical simulations are presented. The simulations successfully predict the results of the experiments in the cases of both the hexagonal and the triangular lattices. The concept of controlling thermal expansion with composite lattice-based materials and structures is therefore proven to be feasible.

Shown in Figure 25a during the experiment, the hexagonal lattice material designed to have zero thermal expansion and maximum specific stiffness exhibits a measured CTE of $\alpha_1^{\mathrm{B}} = 8.5 \times 10^{-6}\,\mathrm{K}^{-1}$—greater than zero but still clearly validating the approach of tuning the elastic properties of each phase by altering the geometry of the hexagonal unit cell. The effective thermal expansion of the composite lattice material is only one half of that predicted for a layered composite material composed of solid layers of aluminum and titanium (Figure 25b). The low thermal expansion of the composite is enabled by combinations of constituent elastic constants that cannot be attained with isotropic solid materials. The effective Poisson's ratios of the A cells and B cells is $\nu_{12}^{\mathrm{A}} = -2.12$ and $\nu_{12}^{\mathrm{B}} = 2.03$, respectively, both substantially outside the thermodynamics limits for isotropic elastic solids, $-1 \leq \nu_{\mathrm{s}} \leq 0.5$.

The non-zero thermal expansion of the sample is due to three factors, each examined in detail previously in Section 5.1: 1) the small relative thickness of the sample, $t^{\mathrm{plate}}/H^{\mathrm{cell}} = 2$, causes the occurrence of a state of predominantly plane stress, not generalized plane strain; (2) the small relative width of the sample, $W^{\mathrm{plate}}/H^{\mathrm{cells}} \approx 7$, causes the presence of the free surfaces to affect significantly the macroscopic response of the sample; (3) the thin aluminum interlayers separating the titanium foils increase the thermal expansion of the B layers. The role of these factors was verified by conducting a simulation with plane stress boundary conditions, plate dimensions identical to those of the sample, and thin aluminum interlayers within the B layers. The CTE predicted by this simulation agrees with the CTE measured in the experiment (Figure 25b), confirming the analysis of the mechanics underlying the macroscopic thermal response. The first two factors are effects only of scale and would not be significant in thicker, wider samples. However, for thin, small samples, these factors can easily be accounted for and included in the analytical and numerical models. For example, using the analytical model with the assumption of plane stress boundary conditions, we find that the geometry that eliminates thermal expansion while maximizing specific stiffness in bending at $t/H^{\mathrm{cell}} = 0.064$ is $h^{\mathrm{A}}/l^{\mathrm{A}} = 1.25$, $\theta^{\mathrm{A}} = -25.4°$, and $\theta^{\mathrm{B}} = 26.6°$. In this case, the Poisson's ratio of each layer, $\nu_{12}^{\mathrm{A}} = -2.19$ and $\nu_{12}^{\mathrm{B}} = 2.09$, is just slightly larger in magnitude than it is in the case of generalized plane strain, and as a result the maximum specific stiffness $\overline{E}_2^{1/3}/\overline{\rho}$ decreases by less than 7%.

The effective thermal expansion of the negative CTE hexagonal sample (Figure 13b) was also successfully measured. This sample exhibited an initial CTE of $\overline{\alpha}_2 \approx -20 \times 10^{-6}\,\mathrm{K}^{-1}$, similar to the model prediction, but further fracture of cell walls occurred after only a small increase of

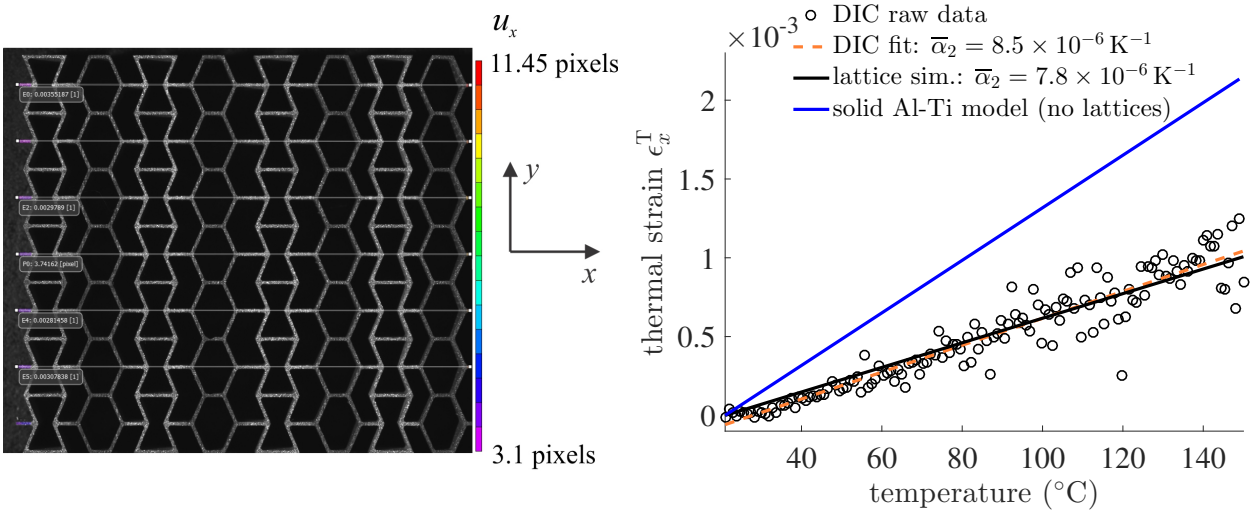

(a) (b)

Figure 25. Measurement of the effective thermal expansion, $\overline{\alpha}_2$, of the composite hexagonal lattice material designed to exhibit both zero thermal expansion and maximum specific stiffness in bending: (a) The total elongation of the sample in the x-direction during heating to 150°C was measured at seven locations; (b) Positive thermal expansion occurred because the thickness and width of the sample are small compared to the height of the cells, H^{cell}, and because the aluminum interlayers within the B layers expand more than the titanium foils do. The measured $\overline{\alpha}_2$ agrees with the prediction of the simulation that accounts for the effects of thickness, width, and interlayers. Although zero CTE was not achieved, the sample exhibited a CTE 50% lower than the CTE predicted for a layered composite of solid aluminum and titanium, validating the approach for controlling CTE.

temperature. The test was therefore immediately stopped. We will attempt to repair all broken cell walls before testing this sample further. The broken cell walls were caused by voids and poorly bonded layers that were present in some sections of the 3D printed composite plate. Including a light stress relief step after printing about every 10 mm in height should minimize these defects and prevent cell walls from breaking during future builds. (Much of the plate was free from defects even without any stress relief.)

The measured response of the composite triangular lattice structures ranges from a large negative CTE to a large positive CTE as the aspect ratio of the triangular unit cell (proportional to b/a) increases (Figure 26). Summarizing the experimental results and model predictions in Figure 27, we demonstrate the accuracy of the numerical models and show that the effective thermal expansion increases nonlinearly with increasing cell wall internal angle, θ. These results agree with the predictions of the analytical model of Equation 6 and indicate that zero thermal expansion can be attained at about $\theta = 35°$. We estimate this angle from the shape of the trend in Figure 27 and

the predictions of the analytical model plotted in Figure 7a. Because the diagonal elements (legs) of the triangular lattice structures are composed of both titanium and aluminum, the ratio of base expansion, $\delta a/a$, to diagonal expansion, $\delta b/b$, in the unit cell is only about 1.6, limiting zero or negative CTE to small angles and low unit cell aspect ratios. At $\theta = 35°$, the triangular unit cell will exhibit a significant degree of anisotropy, and the stiffness will be larger in the 1-direction than it is in the 2-direction.

However, the isotropy and biaxial structural efficiency of the triangular lattice structures can be increased appreciably by optimizing the printing of the composite plate specifically for the manufacture of this type of structure. Printing the base elements from aluminum and the legs entirely from titanium would increase the ratio of base expansion to diagonal expansion to its material limit of $\alpha_{\mathrm{Al}}/\alpha_{\mathrm{Ti}} = 2.75$. In turn, the cell wall internal angle at which zero thermal expansion is predicted to occur would increase to $\theta = 53°$ (Figure 7a). At this angle, the mechanical response of the unit cell would be nearly isotropic, and the structure would exhibit uniaxial and biaxial stiffnesses that are close to the theoretical upper bounds. The density of the structure would be only about $600\,\mathrm{kg/m^3}$ for an intermediate cell wall aspect ratio of $t/H = 0.06$ (Figure 7b). A lightweight structure with both zero CTE and high stiffness could therefore be manufactured with robust, practical methods.

Finally, we note that in none of the experiments, for either type of lattice material, was there evidence of failure by yielding or buckling. Zero or low CTE materials composed of constituent phases with contrasting CTEs exchange stress-free macroscopic expansion or contraction for the generation of internal stresses. If the aspect ratio of the structural elements is too high, then yielding or buckling can occur as the temperature changes, and the mechanism for controlling thermal expansion will cease to operate. However, all the samples showed a linear response during the $120\,°\mathrm{C}$ temperature ramp from room temperature, indicating that neither yielding nor buckling will occur in structures of similar density.

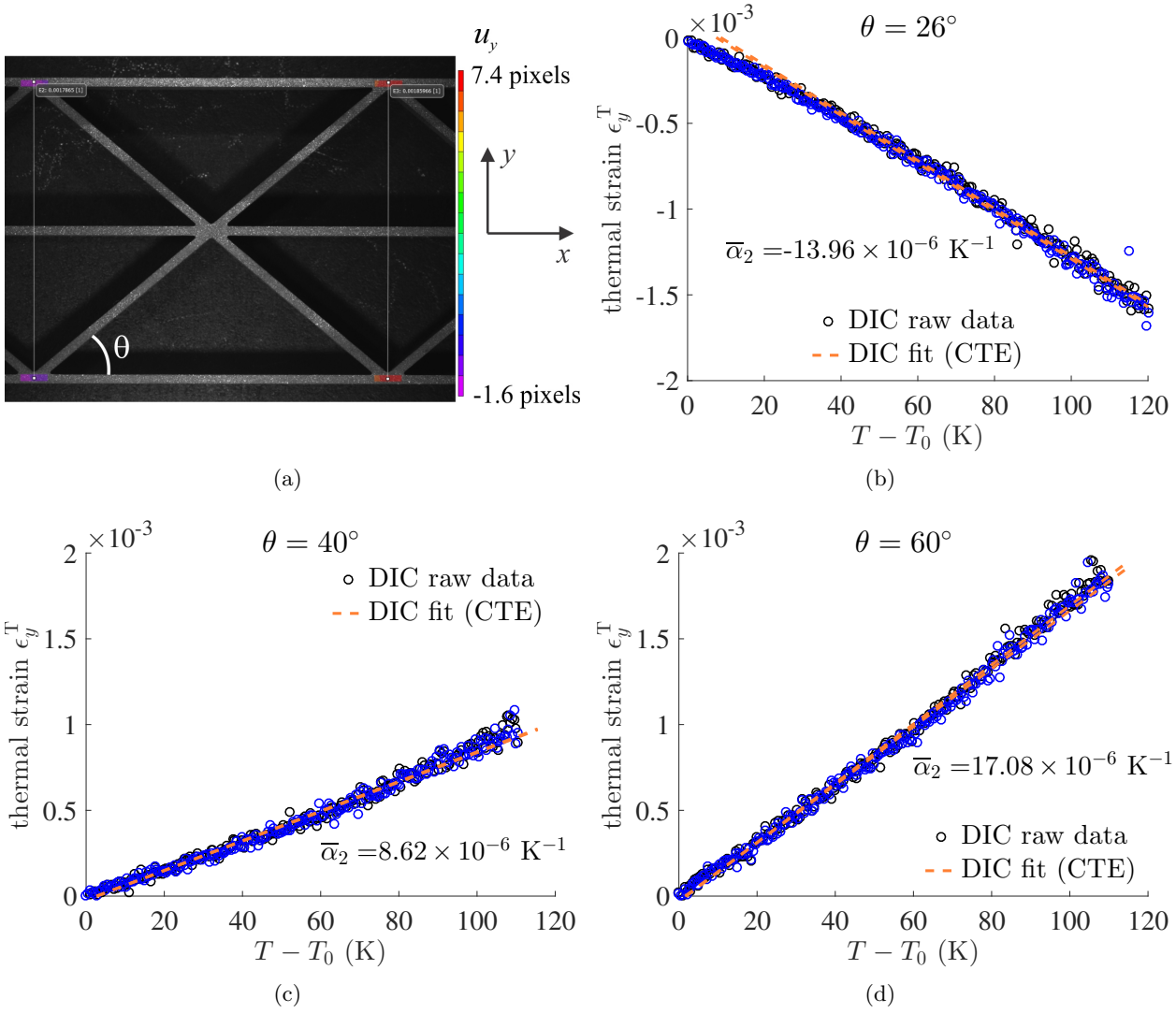

Figure 26. Measurement of the effective thermal expansion, $\overline{\alpha}_2$, of the composite triangular lattice structures: (a) The total elongation of the sample in the y-direction during heating to 140°C was measured at two locations (shown is the structure with cell wall internal angle $\theta = 40\,°$C); (b) At $\theta = 26\,°$C, the thermal expansion is negative, $\overline{\alpha}_2 = -13.96 \times 10^{-6}\,\mathrm{K}^{-1}$; (c) Increasing the cell wall internal angle to $\theta = 40\,°$C causes the thermal expansion to become positive, $\overline{\alpha}_2 = 8.62 \times 10^{-6}\,\mathrm{K}^{-1}$; (d) Increasing the cell wall internal angle to $\theta = 60\,°$C causes the thermal expansion to increase further to $\overline{\alpha}_2 = 17.08 \times 10^{-6}\,\mathrm{K}^{-1}$.

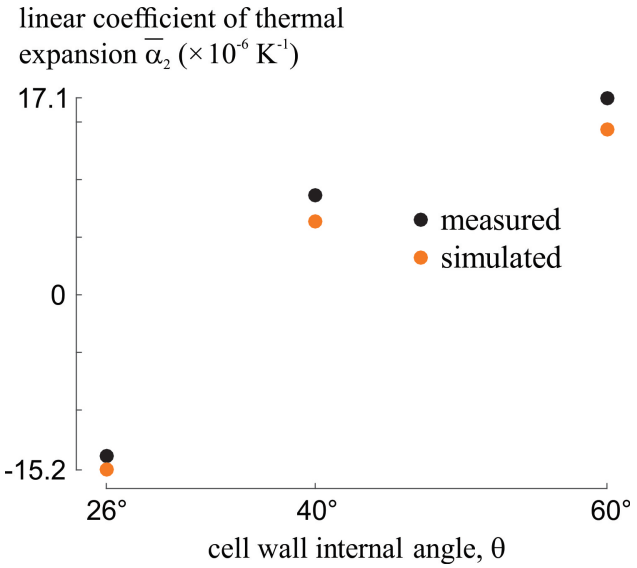

Figure 27. The effective thermal expansion, $\overline{\alpha}_2$, of the composite triangular lattice structure can be broadly tuned by changing the cell wall internal angle, θ. The thermal expansion increases from a negative value of significant magnitude (nearly twice the CTE of titanium) to a sizable positive value as θ is increased. The results of numerical simulations agree with the measurements, proving that the models can be used to tune the thermal expansion of these materials.

6. CONCLUSION

In this document, we describe the modeling, manufacturing, and testing of two types of lightweight cellular metal that exhibit zero and tunable thermal expansion. Both types of material are based on the tessellation of a lattice-based unit cell composed of two materials with contrasting coefficients of thermal expansion. In each case, the superposition of the two constituent materials can result in a composite material with zero effective thermal expansion. In one case, the lattice is hexagonal, and zero thermal expansion results from the competition between thermal expansion and the Poisson effect; in the other case, the lattice is triangular, and zero thermal expansion stems from the inward rotation of lattice elements. Analytical and numerical models predict that the effective response of both types of lattice material can be broadly tuned from negative thermal expansion to positive thermal expansion. With the hexagonal lattice, modeling shows that materials can be designed with zero thermal expansion in one direction, controllable thermal expansion in a second direction, and a structural performance index superior to the indices of conventional aerospace materials such as aluminum and Invar. With the triangular lattice, scaling relations and model predictions indicate that zero thermal expansion can be achieved at specific stiffnesses that surpass by a wide margin those of the hexagonal lattice due to the high nodal connectivity and inherent structural efficiency of the triangular lattice. Samples of both materials were successfully manufactured by 3D printing and computer-controlled machining. In experiments, thermal expansions ranged from $\overline{\alpha}_2 = -14.0 \times 10^{-6}\,\mathrm{K}^{-1}$ to $\overline{\alpha}_2 = 17.1 \times 10^{-6}\,\mathrm{K}^{-1}$, validating the approaches for controlling thermal expansion and verifying the accuracy of the models. Although cellular metals with zero or negative thermal expansion have been proposed before, to our knowledge, these materials are the first lightweight, zero thermal expansion metals that can be manufactured with practical, automated methods at useful scales. Materials that possess this unique combination of tunable, low thermal expansion and high specific stiffness will be valuable in many applications, including thermal interface materials for electronics and optical components, the support structures of precision optical instruments, hypersonic vehicles, and systems for atmospheric reentry.

The capability demonstrated here to design materials by changing underlying structure, rather than simply by selecting from existing materials, can provide new design flexibility and increase the performance and service life of many MIT LL prototypes. Applications are not limited to those requiring low thermal expansion. Similar methods can be used to design hierarchical materials for many other functions, including energy absorption, shock or vibration damping, actuation, morphing, electrical conduction, thermal insulation, and heat dissipation. Furthermore, with the increasing use of miniaturized systems, such as UAVs and CubeSats, size and weight constraints are continually becoming more stringent, intensifying the need for lightweight, engineered materials than can perform multiple functions, such as structure, transport, energy storage, and logic.

This page intentionally left blank.